Modeling and Control of Hybrid Energy Storage Systems on a Hybrid Super Sports Car

Modeling and Control of Hybrid Energy Storage Systems on a Hybrid Super Sport Car

Author, co-author (Do NOT enter this information. It will be pulled from participant tab in MyTechZone)
Affiliation (Do NOT enter this information. It will be pulled from participant tab in MyTechZone)

Abstract

Today, the contribution of the transportation sector on greenhouse gases is evident. The fast consumption of fossil fuels and its impact on the environment have given a strong impetus to the development of vehicles with better fuel economy. Hybrid electric vehicles fit into this context with different targets, from the reduction of emissions and fuel consumption to performance and comfort enhancement. Vehicles exist with various missions; super sports cars usually aim to reach peak performance and to guarantee a great driving experience, but great attention must also be paid to fuel consumption. According to the vehicle mission, hybrid electric vehicles can differ in the powertrain configuration and the choice of the energy storage system. The electrical energy source often consists of batteries, but also capacitors could be used. The energy storage systems could be limited in energy or power density, depending on their technology. This work explores the hybridization of a super sport car by fitting two electric machines in position P2-P4. In addition, even the energy storage system is hybridized by combining batteries and capacitors to get the benefits of both. At first, the hybrid energy storage system is obtained connecting batteries and capacitors in parallel. The research activity shows that such a system could significantly reduce the peak current requested to the batteries and reduce the battery voltage variations, consisting of a simple solution. Later, the connection between capacitors and batteries is regulated by a DC-DC converter, to fully use the capacitors' available energy and to actively control the system. Both the systems are modeled in MATLAB/Simulink and they are eventually introduced as part of a hybrid electric vehicle model. The model is simulated on emission cycles and the fuel consumption results are compared with the ones of the conventional super sport car to determine the improvements on fuel economy.

Introduction

Literature Review

Nowadays, the climate change phenomenon is widely studied and possible solutions to the problem are proposed in various fields, among others the automotive sector. The automotive sector has focused on the improvement of existing technologies and on new proposals focused on the reduction of CO2 emissions [1–4]. Now, the electrification process is trending since electric vehicles (EVs) and hybrid electric vehicles (HEVs) can reduce the fossil fuels consumption with performance comparable to the ones of conventional internal combustion engine (ICE) vehicles [5,6]. On one side, electrification is seen as a great opportunity to challenge climate change, especially in some aspects of road transportation [7]. On the other side, it brings along some issues related to the technologies, that have not yet been overcome [6,8].

One of such issues is represented by the energy storage energy and power density. Different energy storage systems can achieve different performance, for example batteries work well at supplying low and steady loads but are inefficient at high charge/discharge rates that impose severe stress and reduce the battery life span [6–9]. On the other side, capacitors are characterized by a long life cycle and high-power density but have the great disadvantage of a lower energy density [6,8,10–12].

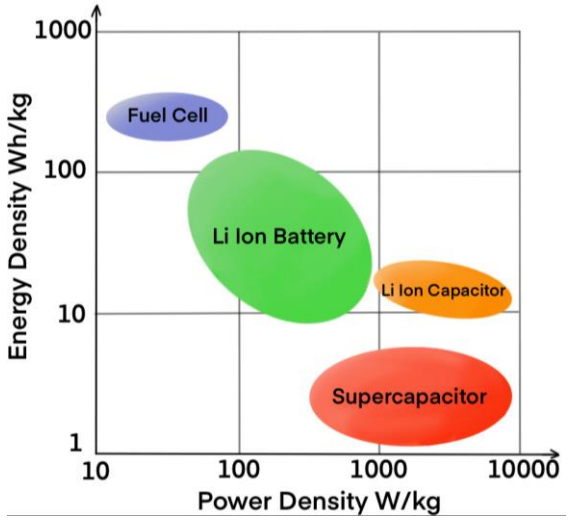

Figure 1. Ragone plot of various energy storage systems [13].

As shown in Figure 1, the Ragone plot illustrates how different energy storage technologies relate one to another; the reader is referred to [13] for further reference. It is evident that capacitors are associated with higher power density values and lower energy density values with respect to batteries. Lithium-Ion Capacitors (LiCs) represent a hybrid solution that achieves higher energy density values than common capacitors, reaching approximately $5 - 13\ Wh/kg$ [13], while Li-Ion batteries typically reach $100 - 250\ Wh/kg$ [14]. The idea that is explored in this work is the design of a Hybrid Energy Storage System (HESS) capable of combining two different technologies to enhance their strengths and peculiarities, while compensating for the disadvantages.

LiCs are derived from Electric Double Layer Capacitors (EDLC) [6], they combine the activated Carbon cathode of an EDLC with the Li-doped Carbon anode of Lithium-Ion Batteries, to guarantee both power and energy. In common automotive applications, they are adopted only for few operations, like Start&Stop [15], and, since it is considered difficult to use capacitors alone as an energy storage reservoir [6,16], they may be used as auxiliaries in combination with other energy

storage systems (Lithium-Ion Batteries, Fuel Cells, …) [17–19]. The HESSs allow to decouple the specific energy and specific power requirements, and while the capacitors could cover the power request, the battery-based energy storage system can be optimized for the energy request and life cycle. Li-Ion Batteries are usually introduced as energy storage reservoir and they are commonly installed in HEVs and EVs due to the high energy content that they can provide [20] (meaning a high electric range in automotive applications). On the other side, they cannot guarantee high power performance [6,21]. Lithium-Ion Batteries are commonly modeled as in [9,22], by choosing the level of complexity that is needed.

Capacitors and batteries could be combined in series or parallel configuration to generate a HESS. With respect to this, various configurations exist [6] and the research on this topic has been increasing in the last years [23–26]. A series connection between batteries and capacitors would lead to a high-voltage system where the single cells are run by the same current. In that case, the current and power of the complete system would be limited by the battery in charge and discharge, making the presence of capacitors useless. On the other side, a parallel connection would allow to maintain the same voltage across batteries and capacitors, while the current would be split between the two different packs of cells. Hypothetically, this would allow to run a higher current on the capacitors while respecting the limits of the battery. To this aim, the capacitors could be sized to cover high power requests, while the batteries could be sized to cover the energy request. The parallel configuration between batteries and capacitors is also defined as 'passive' configuration. This is the simplest parallel hybrid configuration that can be conceived.

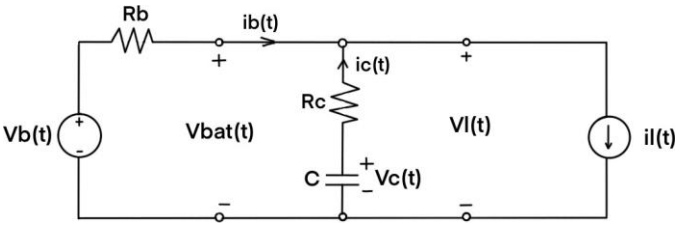

Figure 2. Passive hybrid topology.

In Figure 2 a passive hybrid topology is shown, the reader is referred to [27] for further reference. On the left there is the battery with a terminal voltage $V_{BAT}(t)$, internal voltage $V_B(t)$, internal resistance R_B and a current $i_B(t)$. The battery is connected in parallel with a capacitor characterized by an internal voltage $V_C(t)$, a capacitance C, an internal resistance R_C and a current $i_C(t)$. On the right it is present the load with a terminal voltage $V_L(t)$ and a current $i_L(t)$.

The introduction of DC-DC converters to interface the capacitors and the battery could lead to higher reliability and control flexibility, optimizing the power sharing regarding efficiency. In this case, HESS could guarantee higher performance since capacitors could provide most of the entire pulse load while batteries provide the average and constant part of the load [26,28,29]. When a DC-DC is introduced to interface capacitors and batteries with a parallel connection, the configuration is called 'active' or 'semi-active'. In active and semi-active topology, one or more DC-DC converters are used to control the flow of current to and from the system components. A fully active configuration is one where two DC-DC converters are introduced to interface batteries and capacitors, the reader is referred to [27] for a complete analysis of these configurations. On the other side, a semi-active configuration is one where only one DC-DC converter is used. The alternatives are explained also in [27,30] and for this activity we will refer specifically to the battery semi-active hybrid topology that is represented in Figure 3. The nomenclature of Figure 2 is maintained.

In Figure 3 the converter is located between the battery and the load, connecting the capacitor directly to the load side, $\eta_{DC-DC,BAT}$ is the efficiency of the converter, and $i_{L,AVE}$ is the current flowing from the battery branch.

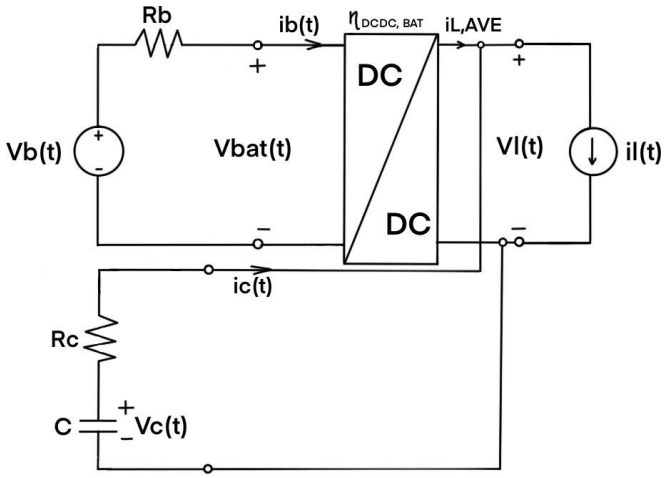

Figure 3. Battery semi-active hybrid topology.

In [26], a comparison between active parallel and series configurations is carried out. It is shown that active hybrids that use two DC-DC converters in series solve problems for capacitors but have a lower global efficiency and they need to add a full-rating DC-DC converter. On the other side, a parallel active configuration solves problems for battery and capacitors but introduces one DC-DC rated at average power and one rated at maximum power bringing complexity, control effort and additional losses. [25] shows that active configurations can guarantee good results for cost saving, since small size capacitors are linked to low costs for power electronics. Still, energy losses in DC-DC converters are usually the main part of the total HESS energy losses [31]. On the other side, a passive parallel configuration allows to work with less electronics and control circuitry, reducing the overall energy, and power density [26,32]. However, a configuration of this kind cannot be actively controlled, and it limits the usable energy of the capacitors, as their voltage must be equal to the battery's terminal one, reducing the system flexibility. As explained in [33], the topology of passive HESS is simple, and saving one or two high-power DC-DC converters will save significant cost for the EV or HEV system. Furthermore, passive HESS performance can be easily improved by choosing capacitors with larger capacitance and smaller internal resistance as it is also shown in [30,34,35]. With the fast development of the capacitor's technology in industry, optimizing the battery and capacitor parameters of passive HESS is a feasible way to improve HESS performance. More importantly, simulation research has been done in [34] showing that passive HESS has a higher energy efficiency than active HESS. For the above reasons, passive HESS still has a great application potential in EVs and HEVs. So, as described in [27], the passive hybrid is the simplest and cheapest technology, the fully active hybrid gives the best performance, compromising cost and simplicity, and the semi-active hybrid is a trade-off between performance and the circuit complexity and price. For our application, a passive HESS and a battery semi-active HESS will be analyzed.

The work done in [8,30] shows how the modeling of a DC-DC converter could be carried out, while the indications in [27] lead to a simpler model that is preferred for our application. Also, [36] explains how fixed ratio DC-DC can lower power dissipation, cut costs, and save size, while [37] shows how fixed ratio DC-DC converters can be optimized for high efficiency, and it illustrates some specific applications. In [38] fixed-ratio DC-DCs are adopted to satisfy the need for high power and high efficiency systems. So, the introduction

of a fixed ratio DC-DC could guarantee comparable performance, saving complexity. The presence of the DC-DC converter allows to control the system guaranteeing high flexibility.

In recent years, researchers have explored various energy management strategies for the HESSs, which can be divided in online and offline strategies [39–41]. The online strategies can be easily implemented in real-world controllers, but generally do not achieve optimal results. In comparison, offline strategies can achieve a globally optimal performance, but they cannot be introduced in real-time applications due to the long computational time, high memory resources requirement, and complete knowledge of the driving conditions [42]. Some common techniques reported in literature for designing an online energy management strategy include rule-based [43], fuzzy logic [44,45], filtering [44]. Offline techniques as dynamic programming can be used as a benchmark for optimal performance as in [46]. Other optimization-based energy management strategies are related to the use of neural networks-based algorithms [47,48] or reinforcement learning [49,50]. To cover the gap between offline optimization and online application, also model predictive control-based strategies could be introduced as in [51]. The current paper focuses on real-time oriented models, that must be compatible with the implementation in the control unit on the real car. This makes rule-based and, more in general, online strategies fit for our application.

Research Project Contribution

The current research project is based on the work done in [52,53], where a super sport HEV, that is associated with higher than typical power requirements, has been modeled and validated. In [52] the conventional super sport car was modeled and experimentally validated. Then, it was modified to reproduce the behavior of a super sport HEV prototype by introducing a high-power density energy storage system (LiCs) controlled by a strategy that was aiming at comfort and performance. In [53] the super sport HEV powertrain configuration was modified and the capabilities of LiCs were explored through the development of various hybrid control strategies. For the current paper, the configuration of [53] is set as a starting point, and the HEV is fitted with two electric machines (EMs) in P2-P4 position.

This paper focuses on deepening the study of the energy storage systems and their impact on the vehicle's longitudinal performance and fuel consumption. The past works have shown how a high-power density can guarantee performance, comfort, and fuel economy. However, the fuel consumption reduction that is achieved is limited because of the small energy content of the LiCs. Therefore, this paper focuses on exploring new energy storage systems that give priority to the power content, because of the characteristics of the vehicle that is chosen, but that are capable also to guarantee a greater energy content.

The literature review leads to assess the possibility of creating a passive and a semi-active HESS, since a hybrid solution could help in overcoming the limits related to the single energy storages. The current paper focuses on the modeling and experimental validation of Li-Ion batteries in a MATLAB/Simulink environment; then, it focuses on the modeling of HESSs by integrating LiCs (already validated in [52]) and Li-Ion batteries and introducing a DC-DC converter. The integration of experimentally validated models and the introduction of the HESSs in a super sport HEV model represent the major contribution of this research project. This kind of activity is particularly indicated for the concept phase of the project, since the physical HESS does not yet exist, and predictions can be made only through modeling and simulations.

A tool of this kind allows to predict and quantify the effects of proposed changes in the systems' characteristics and parameters with major flexibility. Various design proposals can be analyzed with easiness and without the need for a prototype. This possibility is of great importance, since it allows to assess the characteristics of this technology at very low cost. Moreover, it allows to assess its behavior also as a part of the HEV, which would be a very expensive activity if a vehicle prototype was required. On the other hand, this means that the HESS model is not validated in its entirety at the moment; for this type of activity an experimental testing environment could be foreseen.

Methods

The energy storage systems that have been analyzed consist of the LiCs and the Li-Ion batteries. These energy storage systems have been experimentally tested in the lab and the data have been used to determine the models' parameters. Once the single models are completed and validated, the possibility to combine LiCs and batteries in a single system is explored. According to the literature review, a passive HESS and a semi-active HESS are modeled. As previously explained, the passive HESS is based on the parallel connection of the energy storages, while the active HESS introduces a DC-DC converter and a proper control strategy. The DC-DC converter model and its control are based on the work done in [27] and [31,54], where the average power load is determined and supplied by the battery, while the peak power request is satisfied by the LiCs. This allows to achieve a nearly constant battery current, to guarantee performance improving. Moreover, a second control strategy that aims to maintain the battery terminal voltage equal to the load voltage is introduced for a fixed ratio DC-DC. Therefore, the modeling activity for the HESSs is mainly an integration in a MATLAB/Simulink environment of the models of LiCs and batteries that have been individually validated. The HESSs are then tested as a part of the entire super sport HEV model.

The complete HEV is tested on emission cycles and the results are compared with the ones obtained for a conventional vehicle and the ones obtained for a HEV whose energy storage system is based only on capacitors as in [53]. The fuel economy optimization will be one of the assessment parameters and the vehicle model will serve as the basis of the activity. The vehicle model is tested on a WLTC Class 3b, as the one reported in Figure 4. The control strategies that are chosen to power the vehicle are a rule-based strategy (RBS) and an equivalent consumption minimization strategy (ECMS) and the reader is referred to [53] for the complete theoretical explanation. Due to the possible difference between the initial and final energy of the energy storage systems, a fuel consumption correction procedure is introduced. At last, the semi-active configuration is tested for performance. In particular, a HESS is specifically designed to achieve full energy recuperation during a 200-0 km/h braking and then the hybrid powertrain is tested for a 0-200 km/h acceleration.

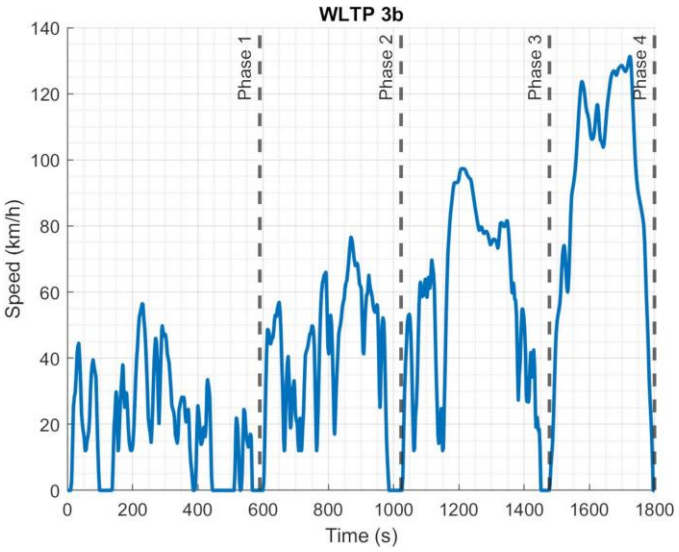

Figure 4. WLTC Class 3b.

Longitudinal Dynamics Model

The longitudinal dynamics vehicle model from [53] reproduces the behavior of a super sport HEV. It considers the WLTC Class 3b speed cycle as input, and it is composed of a proportional-integral controller acting as the accelerator and brake pedals, an engine model subsystem, the gearbox model, the tire model, the electric system, the vehicle resistances, and the longitudinal dynamics equations. The speed cycle input allows to compute at every simulation step the load profile for the vehicle, depending on the vehicle resistances that were experimentally determined or modeled, as explained in previous works [52,53]. Depending on the speed target input and the actual speed, the proportional-integral controller determines an overall torque request to the wheels, which is then split between the ICE and the EMs.

The powertrain configuration that will be adopted is the P2-P4, where the P4 EM will power the front axle and the P2 EM will power the rear axle. For the modeling, validation and further analysis of the conventional model, the reader is referred to [52,53]. The HEV model has been designed for real-time oriented applications, therefore the control strategies that have been adopted for the HEV, to split the torque request between ICE and HESS are the ones previously introduced in [53], and it will be possible to analyze both the RBS and the ECMS behaviors.

Control Strategies

The hybrid control strategies that are adopted were introduced and explained in [53]. These control strategies split the torque request between the ICE and the EMs, and they were modeled and optimized for a single energy storage system. The RBS is a control strategy based on fixed mathematical rules and in our work, it powers the vehicle through purely electric traction when the state of charge (SoC) of the energy storage system is above a certain value (90%), while it deactivates the electric traction when the SoC is below 30%. The regenerative braking function is always active, and it allows to recover energy during braking phases.

The ECMS is a sub-optimal strategy that targets the minimization of the instantaneous equivalent fuel consumption value. The equivalent fuel consumption is determined by summing the thermal engine fuel consumption, which is obtained through interpolation of fuel consumption maps, and the electrical energy equivalent consumption, that is calculated starting from the electrical power request and a specifically designed cost function. The equivalent fuel consumption is calculated instant by instant and it is minimized by splitting the requested torque at the wheels between the thermal components and the electrical ones in the best way possible.

Energy Storage Systems

Lithium-Ion Capacitor

The LiC model is based on the ones introduced and validated in the previous works [52,53]. The scheme is made of a series resistance and a capacitance, making the model simple but accurate enough to reproduce the real behavior, as shown in Figure 5.

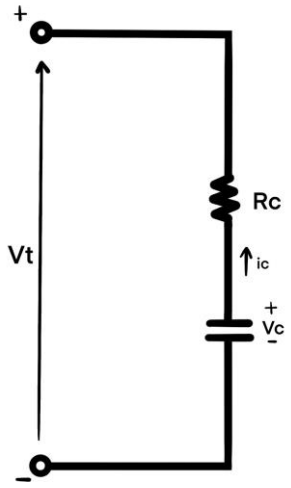

Figure 5. RC circuit for the LiC model.

The introduction of RC branches into the model would make the system more complicated and accurate, as shown in [55], where 8 different parameters control the system's behavior through 4 different branches. This kind of configuration focuses on the reproduction of fast, medium, and slow transients, where the medium and long transients' effects can be noticed over respectively 100 s and 1200 s at null current. As shown in [52], industrial capacitors are focused on the fast capacitance term, maintaining low values for the medium and slow terms. Moreover, for road applications on HEVs where the power request is constant and constantly varying, the effects associated with medium and slow transients are not visible since they would require a long resting time of the capacitor at null current. Due to these motivations, these terms are negligible and the choice to work with a single RC circuit branch is justified. The model has been experimentally tested and validated thanks to data coming from real driving conditions, and the reader is referred to [52,53] for further explanations.

The two EMs fitted on the vehicle express a maximum power of 130 kW. The LiCs are dimensioned to reach that power value, and that is possible thanks to a 60s1p (60 series cells and 1 parallel string) configuration that stores 0.26 kWh. The working voltage spans from 132 V to 228 V.

Lithium-Ion Battery Model

The Li-Ion Battery that has been chosen is a 21700-battery cell (Molicel, INR-21700-P42A) [56]. The model is a double polarization (DP) [9,57] model, made of two RC branches and an internal

resistance, as shown in Figure 6. The decision to work with a DP battery model allows to accurately describe the charge/discharge phenomena. The first RC branch is associated with short transients, while the second one is associated with long transients.

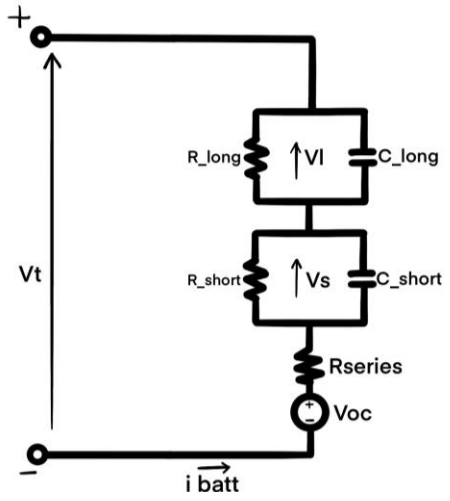

Figure 6. Battery model scheme.

The equations that describe the model are reported, where V_{batt} is the voltage at the battery terminals, I_{batt} is the current flowing through the battery, V_{OC} represents the Open Circuit Voltage, while the R_{series} term indicates the equivalent series resistance and reproduces the sudden effects of a current variation. V_S and V_L respectively indicate the short and long transient voltages, and R_{short}, C_{short}, R_{long}, C_{long} refer to their resistance and capacitance:

$$V_t = V_{OC} - R_{series} \cdot I_{batt} - V_S - V_L \tag{1}$$

$$\frac{dV_s}{dt} = -\frac{V_s}{R_{short} \cdot C_{short}} + \frac{I_{batt}}{C_{short}} \tag{2}$$

$$\frac{dV_L}{dt} = -\frac{V_L}{R_{long} \cdot C_{long}} + \frac{I_{batt}}{C_{long}} \tag{3}$$

The state parameters of the battery are the capacity and the SoC. The capacity of a battery is the amount of electric charge that the battery can store, it depends on the discharge conditions because of the chemical reactions happening within the cells. For a battery pack characterized by a nominal capacity C $[Ah]$ and starting from SoC_0, the SoC can be calculated as follows at a generic instant t, where i is the current flowing in the pack:

$$SoC = SoC_0 - \frac{\int_0^t i dt}{C} \cdot 100 \tag{4}$$

The battery cell has been experimentally tested in the lab on a Pulsed Discharge Test (PDT), shown in Figure 7. The PDT performs the discharge of the battery with discontinuous current, allowing rest time at the end of the current steps (current goes back to 0 A). The rest time is needed to reproduce the cell "relaxation" [57,58] and to study the battery behavior during transients.

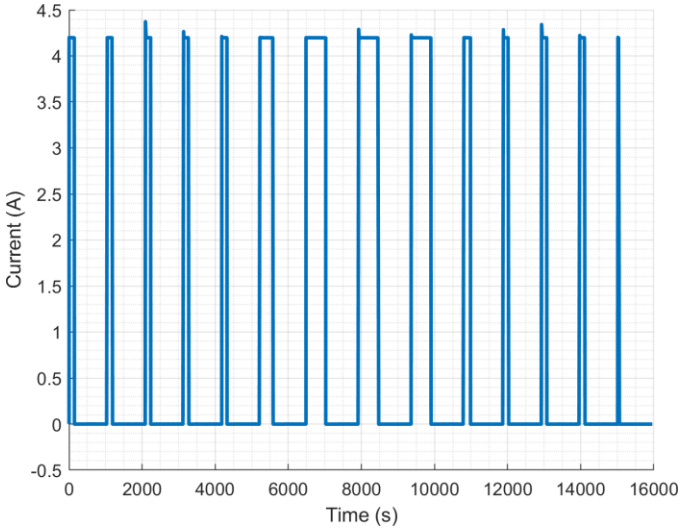

Figure 7. PDT current profile.

The experimental tests take the PDT current shown in Figure 7 as an input and measure the battery voltage variations, that are then reported in Figure 8 under the label 'Experimental'. The study of the voltage profile of the battery allows to determine the parameters needed to complete the battery model, as in [57]. Once the parameters are known and the battery model is complete, it is tested by running a simulation with the current input of Figure 7. This simulation leads to a terminal battery voltage that is reported in Figure 8 under the label 'Simulated'.

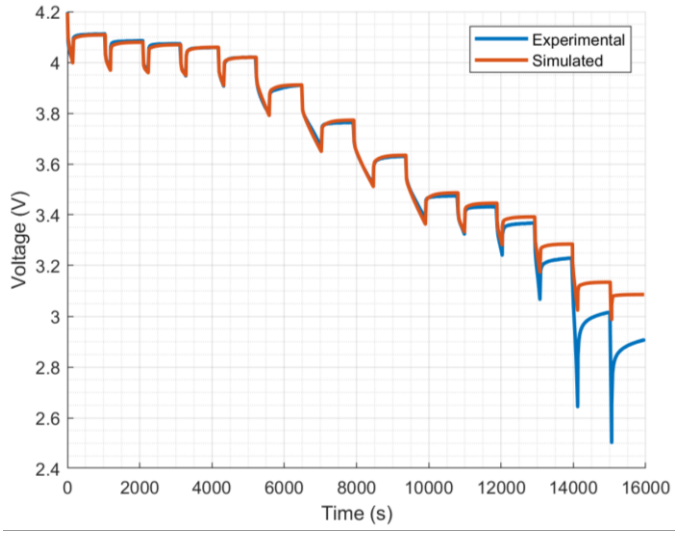

Figure 8. Experimental and simulated terminal battery voltage.

Figure 8 shows that the simulated voltage trend is close to the experimental one, with a root mean square error of 0.07 V. The biggest difference is registered at low voltage when the system reaches its lower limits.

The battery parameters depend on the SoC of the battery pack. However, this dependency is relevant only at very low SoC as it can be seen in Figure 8, where the system will not work during simulations for safety reasons. So, the dependency on SoC is omitted. The battery is also considered to work at ambient temperature, that is maintained constant during simulations, meaning that also the temperature dependency of the parameters is not included in this work. For these

reasons, the battery model is considered reliable and faithful to the real functioning of the system in its field of use.

Passive Hybrid Energy Storage System

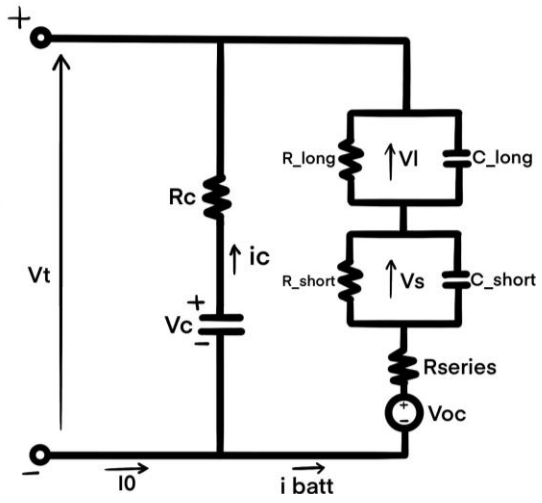

Figure 9. HESS passive scheme.

The first HESS is a parallel passive hybrid, that follows the scheme of Figure 9. The LiCs are dimensioned to satisfy the power request of the EMs. The first hybrid configuration that is here explained sees the introduction of the battery pack in parallel with the LiCs. Therefore, it will be dimensioned to guarantee a similar voltage range by choosing a proper number of cells in series configuration. With respect to the number of parallels, the decision is to work with a single branch, since increasing the number of branches in parallel configuration would lead to an increase in the weight and size of the hybrid pack. The current hybrid pack application is destined to a super sport car and needs to respect stringent limits on size and weight.

Therefore, the battery configuration that has been chosen is a 54s1p (54 series and 1 parallel string) that stores 0.79 kWh and could reach approx. 9 kW of power in discharge phase and approx. 0.8 kW in charge phase. The working voltage spans from a minimum working voltage of 160 V to a maximum voltage of 226 V. The maximum discharge current for a single cell is 45 A, while the charge current is equal to -4.2A. The energy contribution of the batteries is three times the one of the LiCs. The components of the passive hybrid system have been previously described, but the passive HESS needs a deep analysis itself since complexity arises by combining the two systems in parallel. A preliminary analysis was carried out on a simplified system. So, assuming that the battery can be modeled as a single voltage generator and a series resistance, the scheme will be the one in Figure 10:

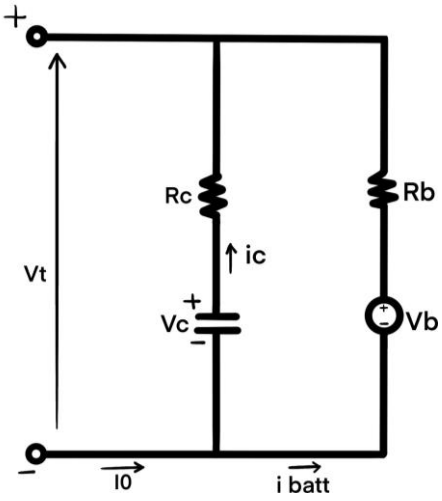

Figure 10. HESS passive simplified scheme.

From this starting scheme, the circuit is derived into the frequency domain and the Thevenin circuit is derived as it can be seen in Figure 11.

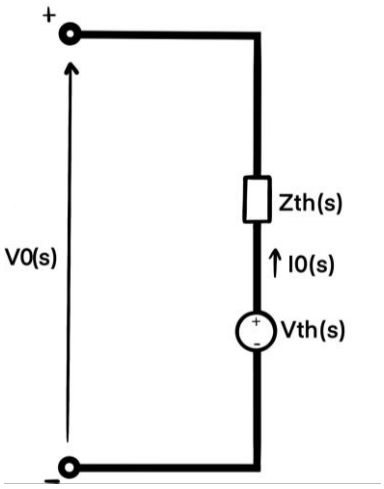

Figure 11. HESS passive Thevenin equivalent circuit.

The reader is referred to [30,34] for the complete theoretical analysis of the system, while here a focus on the results for this specific case is presented. In particular, we obtain:

$$V_{th}(s) = \frac{R_c}{R_b + R_c} V_b \frac{s+\alpha}{s(s+\beta)} + \frac{R_b}{R_b + R_c} V_{c0} \frac{1}{s+\beta} \quad (5)$$

$$Z_{th}(s) = \frac{R_b R_c}{R_b + R_c} \frac{s+\alpha}{s+\beta} \quad (6)$$

Where V_{th} and Z_{th} are respectively the Thevenin equivalent voltage and the Thevenin equivalent impedance, s is the complex frequency, R_c and R_b are the capacitor and battery resistances and V_b is the battery voltage. The capacitor with non-zero initial conditions has been replaced in the Laplace domain by an uncharged capacitor in series with a step-function voltage source with amplitude V_{c0}, $\alpha = \frac{1}{R_c C_c}$, and $\beta = \frac{1}{(R_b + R_c) C_c}$. Eventually, a real load could be applied, however for an analytical approach an ideal pulsed square load is applied to capture the fundamental characteristics and the behavior of the system. The

pulsed load current has a period T, pulse duty ratio D and it can be expressed for the first N pulses as:

$$i_0(t) = I_0 \sum_{k=0}^{N-1} [\Phi(t - kT) - \Phi(t - (k + D)T)] \tag{7}$$

Where I_0 is the amplitude of the current and $\Phi(t)$ is a unit step function at $t = 0$. The equations are passed through the frequency domain and the inverse Laplace transform as shown in [30,34]. Then, the currents of the battery and supercapacitors are determined with respect to the steady-state performance, so when the capacitor and battery voltage are equal $V_b = V_{c0}$. This leads to:

$$i_{b,ss}(t) = I_0 \sum_{k=0}^{N-1} \{\left(1 - \frac{R_b}{R_b + R_c} e^{-\beta(t-kT)}\right) \cdot \Phi(t - kT) - \left(1 - \frac{R_b}{R_b + R_c} e^{-\beta(t-(k+D)T)}\right) \cdot \Phi(t - (k + D)T)\} \tag{8}$$

$$i_{c,ss}(t) = \frac{R_b I_0}{R_b + R_c} \sum_{k=0}^{N-1} \{e^{-\beta(t-kT)} \cdot \Phi(t - kT) - e^{-\beta(t-(k+D)T)} \cdot \Phi(t - (k + D)T)\} \tag{9}$$

Peak Performance

The target is now to simulate the battery behavior to determine the current peak, that occurs at the end of the pulse load $t = (k + D)T$. The battery peak current becomes, for $N \to \infty$:

$$I_{b,peak} = I_0 \left(1 - \frac{R_b}{R_b + R_c} \frac{e^{-\beta DT}(1 - e^{-\beta(1-D)T})}{1 - e^{-\beta T}}\right) = I_0(1 - \zeta_c) = \frac{I_0}{\gamma} \tag{10}$$

ζ_c is the current sharing factor and γ is the power enhancement factor. This means that without a capacitor, the battery would have to meet the peak load by itself, while the hybrid system can supply a higher load than the battery itself. If I_{rated} is the rated current for the battery, the new possible load current of the hybrid system can be expressed as $I_0 = \gamma \cdot I_{rated}$. And the instantaneous peak power becomes:

$$P_{peak} = I_0 V_b = \gamma \cdot I_{rated} V_b = \gamma \cdot P_{rated} \tag{11}$$

The presence of the capacitor allows to make the power enhancement factor larger than one. Considering the eigen frequency of our system for a simplified model $R_b = 1.40\ Ohm$, $R_c = 0.06\ Ohm$ and $C_c = 55\ F$:

$$f_{eigen} = \frac{1}{(R_b + R_c)C_c} = 0.012\ Hz \tag{12}$$

The power enhancement dependency on frequency and duty cycle is plotted in Figure 12:

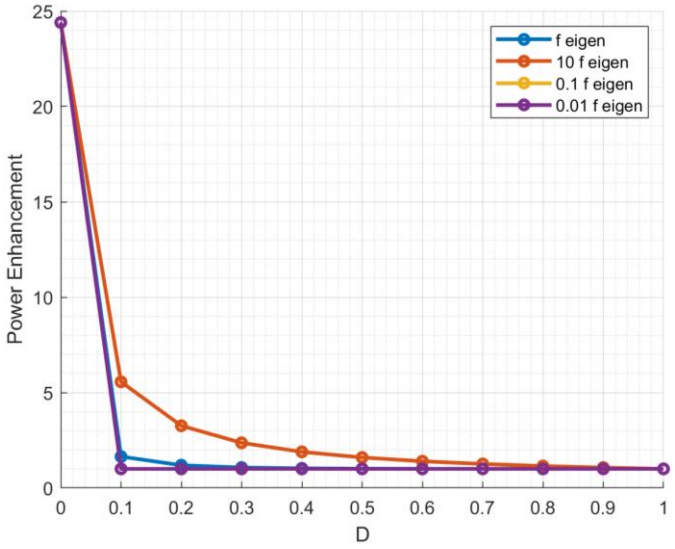

Figure 12. Peak power enhancement dependency on the duty cycle D.

As the frequency grows and becomes way higher than the eigen frequency, the power enhancement reaches a limit close to that of $10 f_{eigen}$. On the other side, the maximum theoretical possible enhancement of output power could be increased 24.4 times the output power of the battery-alone system, as we can obtain for the case of $D = 0$. By lowering the internal resistance, the capacitor is going to give reduced power losses, since it covers a significant share of the output current. Another important information that can be carried out from this analysis is that a passive HESS is not capable of delivering the complete capacitor range of power, reducing the flexibility of the system if compared with a capacitor-only energy storage.

Power Saving

Since the capacitors take a high share of current, the losses depend also on their internal resistance, that is usually lower than that of batteries. This results in lower power losses. A power saving factor ε can be introduced according to the work done in [30,34], and Figure 13 shows the dependency of the power saving factor with respect to the duty cycle D. The reader is referred to [30,34] for the theoretical formulation of the power saving factor.

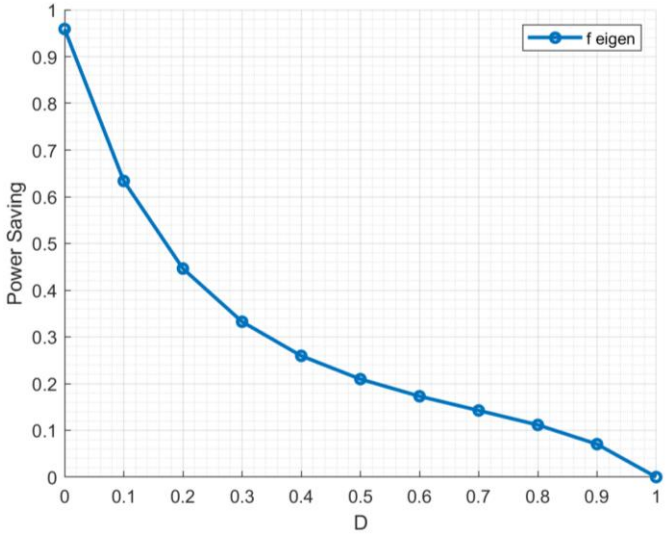

Figure 13. Power saving dependency on the duty cycle D.

If D goes to 1, we approach a constant current and the savings become equal to zero, while the theoretical maximum power saving is given by $D \to 0$:

$$\lim_{D\to 0} \varepsilon = \frac{R_b}{R_b + R_c} \tag{13}$$

Run Time Extension

Since a system of this kind leads to a power saving, a run time extension for the batteries can be obtained. From [30,34] $\Delta\tau = \tau_{hybrid} - \tau_b$ is the extended run time extension of the system due to the reduced losses, while τ_b is the total run time of the battery-alone system (assuming it can run to 100% depth of discharge). And we obtain:

$$\frac{\Delta\tau}{\tau_b} = \frac{\varepsilon\sqrt{D}\delta}{1 - \varepsilon\sqrt{D}\delta} \tag{14}$$

Where $\delta = \frac{R_b I_0}{V_b}$. When $R_b = 0$ the internal voltage drop is zero and the time extension becomes zero because there is no dissipation. On the other side, when the load increases, the dissipation increases and so does δ. If δ is fixed, once the load is known, the run time extension could be evaluated under the variation of D and ε (which depends on D and on the system frequency), as shown in Figure 14.

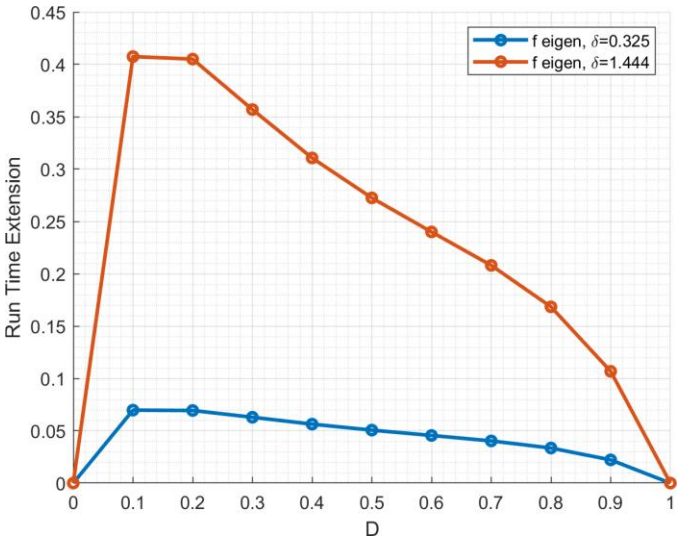

Figure 14. Run time extension dependency on the duty cycle D and on δ.

For $D \to 0$ the run time extension is zero, while the power saving, and the peak power enhancement have a maximum. This is because the system is not utilized when the current is zero. The run time extension goes to zero also when D goes to 1, since the situation is one of constant current and the capacitor are not utilized. The run time extension maximum depends also on the frequency of the pulse load and as the frequency becomes lower, the D associated to the maximum is reduced.

Current Model

For our HESS, a PDT is chosen with $D = 0.2, T = 720\ s, I_0 = 3.4\ A$. A system of this kind is expected to guarantee a $\zeta_c = 0.21, \gamma = 1.26, \varepsilon = 50\%, \frac{\Delta\tau}{\tau_b} = 0.8\%$. This theoretical analysis of a simplified system allows to formulate the expected behavior of the hybrid system. Since the theoretical analysis has been carried out on a simplified version of the model, the results will slightly differ from the expected ones. The model is realized through MATLAB/Simulink and Simscape Power System. A simulation has then been run for the PDT specified previously, and Figure 15 shows the system currents:

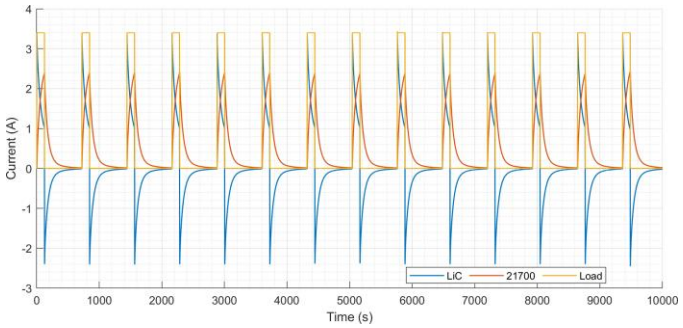

Figure 15. LiCs, battery and PDT current.

In Figure 15 the current load is shown in yellow. As soon as the current request rises to 3.4 A, the HESS is activated and satisfies the current request thanks to the contribution of both the battery and the LiCs. The LiCs power the system in short times due to their high-power values, fulfilling almost all the initial request, while the battery has slower transients. This could be useful during both real driving scenarios and emission cycles as the ones presented in [59], since they are usually characterized by a high variability and they are subject to fast transients.

So, both the battery and capacitors supply current during the load on-state, while the battery charges the capacitors during the load off-state. In this situation, the battery current starts decreasing while the LiCs' current becomes negative to guarantee a sum of currents that is equal to the load request, hence null. Therefore, the instantaneous battery current, which otherwise would be at the same level of the load current request, is reduced considerably due to the assistance of the capacitors that can relieve peak stresses on the battery, and they positively influence the system performance. Figure 16 shows the simulated voltage profile.

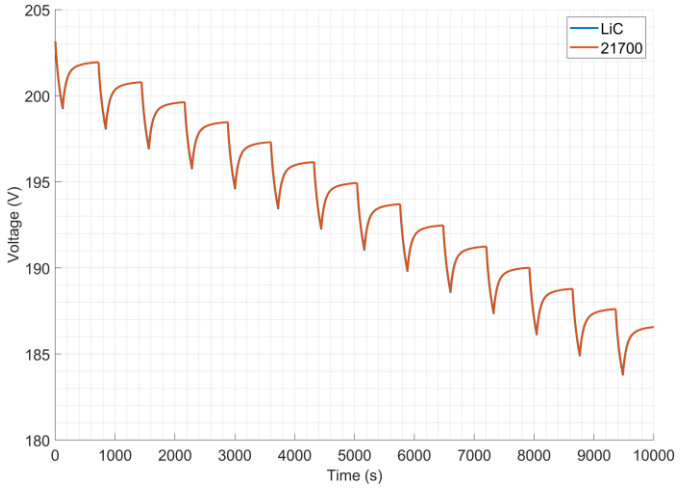

Figure 16. Simulated voltage profile.

Figure 17 shows a comparison between two simulations under the same PDT current input. The voltage profile of the 21700 batteries is shown both for a simulation run for the passive HESS and for the batteries as a stand-alone system. The voltage of the stand-alone batteries reaches values that are lower than the passive HESS, this is

due to the presence of the LiCs in the passive configuration, implying a higher energy content.

The comparison between the voltages in Figure 17 shows that the voltage variation of the batteries as a part of the passive HESS is significantly reduced with respect to the batteries as a stand-alone system. This is due to the lower instantaneous current that runs through the system, as shown in Figure 15. The results demonstrate a significant benefit of the hybridization in reducing the fast and large battery terminal voltage transients as explained in [60].

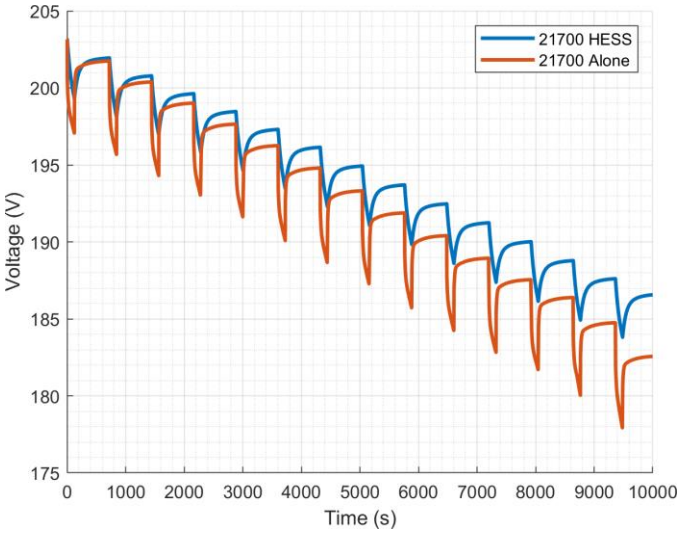

Figure 17. Voltage comparison between a battery stand-alone system and a passive HESS.

It has been verified that for short power pulses the LiCs can supply a large part of the power, reducing the stress on the battery. For longer power pulses, the ratio of the power coming from the battery increases as the voltage of the LiCs drops with theirs SoC. According to the work done in [61], this kind of connection is beneficial when the pulse duration is shorter than 10 seconds and when the power electronic complexity needs to be kept at minimum. A drawback of this configuration is the need to match the voltages of batteries and LiCs, that could become a problem at high voltage. In fact, as explained in [62], a higher energy storage device voltage means the higher potential to have cell imbalances, that could prevent the string from reaching the nominal voltage. It should be kept into account that the usable energy of the LiCs depends on the voltage range of the battery pack. Since the working voltage of the battery is reduced with respect to the one of LiCs, also the energy available from LiCs decreases:

$$E_{LiC} = \frac{1}{2} \cdot c \cdot ({V_{batt,max}}^2 - {V_{batt,min}}^2) \quad (15)$$

Where c is the LiCs' capacitance and $V_{batt,max}$, $V_{batt,min}$ are respectively the maximum and minimum battery voltage.

Control

The passive HESS splits the load current between LiCs and batteries in a nearly uncontrolled manner, determined predominantly by the internal impedances of the system, as shown in equations 8 and 9. Therefore, a control strategy is introduced on the vehicle model to be sure that the current limits of the battery are not exceeded (especially the -4.2 A charge current limit). If the charging limits are exceeded a great quantitative of energy coming from regenerative braking would be lost. The control strategy is the one that follows:

Table 1. Control strategy for a pack that is charging.

$\lvert i_{batt}\rvert < \lvert i_{batt,lim}\rvert$	$i_{HESS,lim} = \frac{V - V_{batt,max}}{R_{batt}} + \frac{V - V_{LiC,max}}{R_{LiC}}$
$\lvert i_{batt}\rvert = \lvert i_{batt,lim}\rvert$	$i_{HESS,lim} = i_{batt,lim}$

The strategy shown in Table 1 implies that as long as the battery current i_{batt} is lower in absolute value than the battery current limit for charge $i_{batt,lim}$, the limit current for the passive HESS $i_{HESS,lim}$ is given by the sum of the current from the LiCs and the batteries to reach their maximum voltages, respectively $V_{LiC,max}$ and $V_{batt,max}$, calculated thanks to their internal resistances, R_{LiC} and R_{batt}. As soon as the battery current reaches the limit, the limit current for the passive HESS will be set equal to the battery limit. This is necessary because in a passive HESS we cannot intervene on the battery control alone as the current share is determined by the internal impedances of the system, as it has been shown previously. Instead, we must deal with the entire energy storage.

Table 2. Control strategy for a pack that is discharging.

$\lvert i_{batt}\rvert < \lvert i_{batt,lim}\rvert$	$i_{HESS,lim} = \frac{V - V_{batt,min}}{R_{batt}} + \frac{V - V_{LiC,min}}{R_{LiC}}$
$\lvert i_{batt}\rvert = \lvert i_{batt,lim}\rvert$	$i_{HESS,lim} = i_{batt,lim}$

The strategy shown in Table 2 implies that as long as the battery current i_{batt} is lower in absolute value than the battery current limit for charge $i_{batt,lim}$, the limit current for the passive HESS $i_{HESS,lim}$ is given by the sum of the current from the LiCs and the batteries to reach their minimum voltages, respectively $V_{LiC,min}$ and $V_{batt,min}$, calculated thanks to their internal resistances, R_{LiC} and R_{batt}. As soon as the battery current reaches the limit, the limit current for the passive HESS will be set equal to the battery limit. This is necessary for the same reason mentioned above.

This control strategy is implemented on the vehicle model, and its impact will be analyzed in the following chapters thanks to simulations on the WLTC Class 3b. In particular, the simulations are run in the Results section. To sum up the analysis that has been run in the previous paragraphs with respect to the passive HESS, it has been demonstrated that the passive HESS is a simple system, that can ensure low weights and small sizes, as well as being inexpensive. However, it has some disadvantages as it needs the voltage of capacitors and batteries to coincide, which means that the capacitors will work in the same voltage range as the batteries, with a consequent limitation on the energy that can be used. In addition, a system of this type presents limited control possibilities. The introduction of a control strategy over the whole passive HESS protects the batteries from over-current but does not make up for the limits related to the range of operation of the capacitors.

Semi-Active Hybrid Energy Storage System

The introduction of one or more DC-DC converters could be seen as a solution to avoid the problems associated with the passive HESS. A semi-active system as the one shown in Figure 3 and Figure 18 is introduced and modeled. The semi-active system is capable of interfacing the capacitors and the battery to achieve higher reliability and control flexibility, and to optimize the power sharing [26,28,29]. The presence of a DC-DC converter allows to control the system and to make use of the full voltage range of capacitors. On the other hand, it implies additional costs, a greater size of the system and a greater

weight. The configuration that has been chosen fits a pack of LiCs in 60s1p configuration (as introduced in the Lithium-Ion Capacitor section) connected to the load, so the configuration that is chosen for further evaluations is a battery semi-active hybrid as shown in Figure 18.

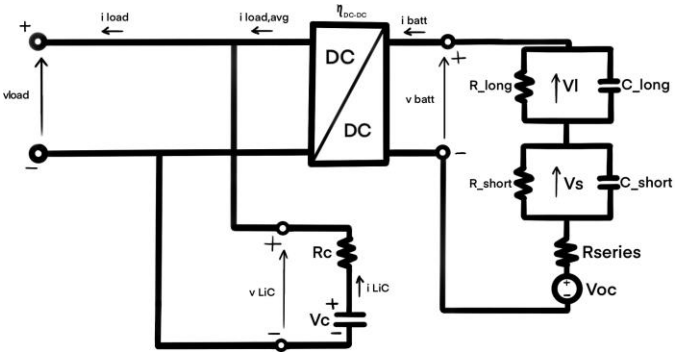

Figure 18. Battery semi-active hybrid energy storage system.

This way, the LiCs' energy storage is directly connected to the inverter and the EMs, while the DC-DC converter is connected between the battery and the load. This configuration allows to dimension the DC-DC converter for the average power flow, keeping the battery current at a near constant value despite the load current variations. As stated in [27], this allows significant battery performance improving in lifetime, energy efficiency and operating temperature. Moreover, voltage matching between battery and load/LiCs is no longer required.

DC-DC Converter

The DC-DC converter could be modeled according to the work done in [8,30], but that level of accuracy is not needed at this point of the work. So, the indications in [27] are followed and a simple system is modeled. v_{batt} indicates the battery voltage, v_{load} the load voltage, k is the conversion ratio, i_{batt} is the battery current, i_{load} is the load current, η_{DC-DC} is the converter efficiency, i_{LiC} is the LiC current.

$$v_{batt} = \frac{v_{load}}{k} \tag{16}$$

$$i_{batt} = \frac{i_{load}}{\eta_{DC-DC}} k \tag{17}$$

$$i_{LiC} = i_{load} - i_{batt} \tag{18}$$

The conversion ratio k is adopted instead of an explicit duty cycle dependent conversion ratio. The value of the conversion ratio is related to the working mode of the DC-DC converter. In boost operation $k > 1$, fewer cells in series can be used to form a battery pack with a terminal voltage lower than the load voltage. This reduces the pack size and the internal resistance. However, as it is explained in [27], in this case the current flowing through the battery pack is higher than the load current, resulting in higher losses due to heating and requiring cells to have higher discharge rate capabilities. When in buck operation, $k < 1$, the battery pack has more cells in series to form a pack with a terminal voltage higher than the load voltage. This would increase the pack size and the internal resistance. In this case the DC-DC converter voltage rating should be chosen according to the maximum voltage of the battery pack. On the other side, the current flowing through the battery pack is lower than the load current, meaning that the losses are reduced, and the cells are required to have lower discharge rate capabilities. For our simulations, the battery voltage could be higher or lower than the load voltage, meaning that the converter is operating in buck or boost mode respectively.

Converter Control Strategy

The choice of the converter control logic is linked with the need for a real-time oriented model, compatible with the implementation on the real vehicle control unit. So, the DC-DC converter control is based on the work done in [31,54], where the average power load is determined and requested to the battery, while the peak power request is satisfied by the LiCs. This allows to achieve a nearly constant battery current, to guarantee performance improving in energy efficiency and operating temperature. In particular, the average load power P_{ave} at instant t is determined thanks to the power load P_{load}:

$$P_{ave} = \frac{\int_0^t P_{load}}{t} \tag{19}$$

That value is then divided by the load voltage v_{load} to determine the $i_{load,avg}$:

$$i_{load,avg} = \frac{P_{ave}}{v_{load}} \tag{20}$$

Then, the battery current i_{batt} is determined as:

$$i_{batt} = \frac{i_{load,avg}}{\eta_{DC-DC}} \tag{21}$$

While i_{LiC} is determined from equation 18. The power load entering the DC-DC model is given by the RBS or the ECMS. The current output for LiCs and batteries will be limited according to the respective limits, in order not to fail the circuit.

Fixed Ratio DC-DC

At last, a fixed ratio DC-DC is analyzed as a substitute of the DC-DC converter, with a fixed ratio equal to 1. This should guarantee comparable performance, saving complexity [36]. The control strategy that is here introduced aims to maintain the battery terminal voltage equal to the load voltage. This should simplify the structure of the fixed ratio DC-DC that is used. A system of this kind is analyzed to verify its feasibility with the target of optimizing the vehicle fuel economy. According to the configuration in Figure 18, the load voltage v_{load} corresponds to the LiCs' terminal voltage, and this value corresponds to the one at the terminals of the battery. Since the battery can be seen as a voltage generator v_{batt} and an internal resistance R_0, connected in series run by a current i_{batt}, we will have:

$$v_{load} = v_{batt} - R_0 \cdot i_{batt} \tag{22}$$

The i_{batt} is determined and the i_{LiC} is equal to:

$$i_{LiC} = i_{load} - i_{batt} \cdot \eta_{DC-DC} \tag{23}$$

A system of this kind is associated with a lower complexity with respect to the previous DC-DC converter solution. The disadvantages that are present when DC-DC converters are adopted are represented by the variations of the load voltage during capacitor charging/discharging, that is strictly related to the fact that the capacitor voltage must match the load voltage.

Results

A conventional vehicle simulation on a WLTC Class 3b was run as a reference. Moreover, the simulations that were done in [53], with a P2-P4 configuration and an energy storage system uniquely based on

LiCs, are reported under the name 'LiC 60s1p'. The WLTC Class 3b cycle phases were defined as follows, as illustrated in [59] and shown in Figure 4:

- Phase 1: 0s – 589s
- Phase 2: 590s – 1023s
- Phase 3: 1024s – 1478s
- Phase 4: 1479s – 1800s

The tables reporting the results show in the first line the conventional series vehicle simulation, while in the following lines they show the simulated results for the HEVs. The fuel consumption simulated results for the conventional vehicle are normalized (%) with respect to the maximum fuel consumption value obtained during the various cycle phases. As it will be shown, Phase 1 is usually associated with the maximum value (i.e. 100%) since the engine works in cold start conditions and at high fuel consumption operating points. The simulated results for the HEVs configurations are reported as a fuel consumption comparison with the series vehicle, showing the percentage reduction.

Fuel Consumption Correction

A fuel consumption correction is carried out, based on the procedure implemented in [7] and explained below. During the cycle, the energy requested at the wheels can be delivered by the ICE or the EMs since we are working with a HEV, therefore two different situations can occur as the energy balance at the end of the cycle, expressed as ΔeC [kJ], could be positive or negative, i.e. the energy storage SoC at the end of the cycle is higher or lower than the initial value.

In the first scenario, it is assumed that the positive difference of the electric energy is covered by the ICE, consuming more fuel than required and recharging the energy storage systems through the EMs that are acting as generators. This means that on the right side of (24 the EM efficiency is at the denominator because the energy content in the energy storage is lower than the starting energy content coming from the fuel. The virtual fuel consumption (to be subtracted to the actual one) is calculated using the average efficiencies of the EMs, as shown in the following equation:

$$\Delta m_{fuel} \cdot LHV \cdot \bar{\eta}_{ICE} = \frac{\Delta eC}{\bar{\eta}_{EM}} \tag{24}$$

Where LHV is the lower heating value of the fuel, and $\bar{\eta}_{ICE}$ and $\bar{\eta}_{EM}$ are the average efficiencies, respectively for the ICE and the EM. In the second scenario, with a negative electrical energy balance, the difference is considered as a further request of torque addressed to the EMs instead of using the ICE. Therefore, it is possible to calculate the additional fuel consumption to be added to the actual one, to compensate the battery balance. The formulation is expressed as follows:

$$\Delta m_{fuel} \cdot LHV \cdot \bar{\eta}_{ICE} = \bar{\eta}_{EM} \cdot \Delta eC \tag{25}$$

Here, the EM efficiency on the right side of (25 multiplies the energy content of the energy storage since the EM is working as a motor, meaning that the energy content of the energy storage is higher than its equivalent in fuel energy. The fuel consumption correction is used to correct the combined final value of the various simulations. When the correction is applied, it will be properly reported.

Passive HESS

RBS

The vehicle is simulated on a WLTC Class 3b with a passive HESS configuration, and the results can be seen in Figure 19 and Table 3. As previously introduced, Table 3 shows the results for the reference configurations given by the Lamborghini Aventador conventional vehicle and by the vehicle configuration with P2-P4 EMs with an energy storage uniquely based on LiCs from [53]. Moreover, the fuel consumption results for the passive HESS are shown. Figure 19 shows the simulation of the passive HESS on an RBS. The LiCs' SoC is chosen as the state variable, therefore the RBS is activated or deactivated when the LiC's SoC reaches the respective target values. This way, every time the electrical driving is activated, the traction power will be guaranteed by the LiCs.

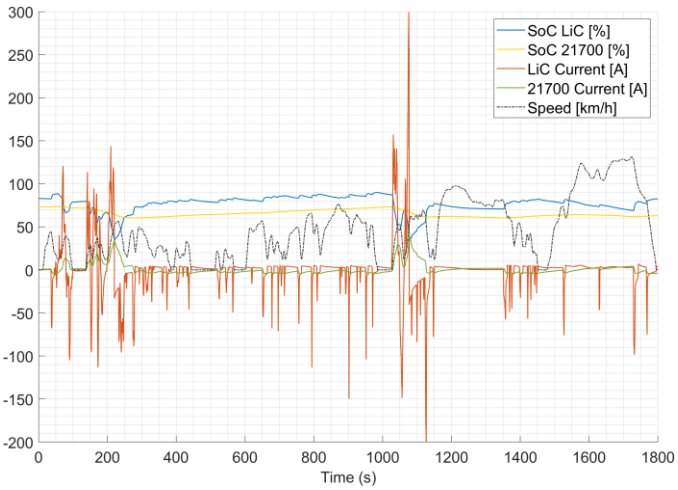

Figure 19. Passive HESS WLTC Class 3b on an RBS.

Table 3. WLTC Class 3b simulated results, for a P2-P4 hybrid configuration with a passive HESS and an RBS.

P2-P4 RBS	Phase 1	Phase 2	Phase 3	Phase 4	Combined	Corrected
Simulated %	100	54	43	41	52	\
LiC 60s1p	-1.2	-7.1	-2.7	+0.6	-2.3	\
Passive HESS	-2.1	+1.5	-3.5	+1.2	-0.7	-0.2

The RBS ensures a reduction of fuel consumption, respecting the HESS current limits. As it can be seen, the fuel consumption is reduced in those phases where the hybrid powertrain is activated, otherwise it increases due to the greater weight. As the final SoC differs from the initial one, the fuel consumption correction is applied. The simulation of an RBS for a passive HESS shows a reduction of approximately -0.2% after the fuel consumption correction. If compared with the value obtained for a LiC-based hybrid powertrain (LiC 60s1p), the passive HESS gets a worse result, making the addition of batteries apparently useless in this case. The major problem of the passive HESS is represented by the fact that it cannot recover all the energy available through regenerative braking due to current limitations introduced for safety reasons through the control strategy presented in [53]. On the other side, a LiC-based configuration does not experience the same current limitations derived from the presence of additional batteries, making it capable of recovering more energy.

ECMS

An ECMS simulation is run to complete the analysis on the passive HESS. The ECMS splits the torque to guarantee the minimization of the equivalent fuel consumption, keeping into account the system's limitations. In particular, the strategy that is here simulated is the

ECMS CS 50%. The ECMS with an SoC depending on speed is not simulated for the passive HESS, as it is not ideal since the direct connection between the battery and the LiCs would make the SoC variation slow and uncapable of following properly the fast variations of the target SoC due to the current limits of the battery. This highlights that the power limit has a major importance for the energy storage systems, especially for super sport cars. The simulation done in [53] is considered for the 'LiC 60s1p' reference. The results are reported in Figure 20 and Table 4.

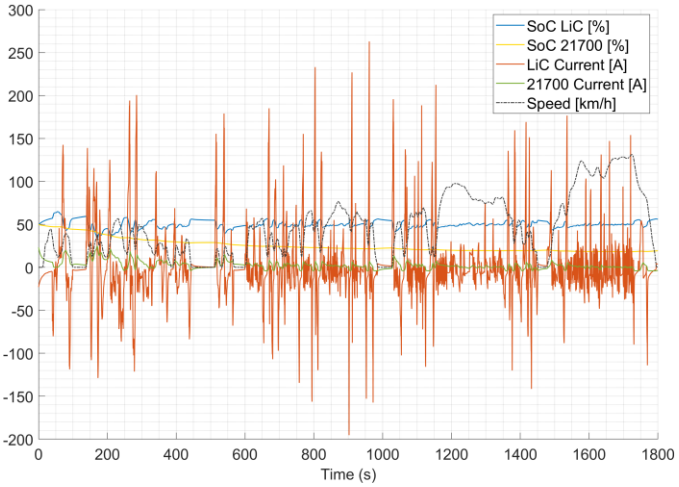

Figure 20. Passive HESS WLTC Class 3b on an ECMS.

Table 4. WLTC Class 3b simulated results, for a P2-P4 hybrid configuration with a passive HESS and an ECMS CS.

P2-P4 ECMS CS	Phase 1	Phase 2	Phase 3	Phase 4	Combined	Corrected
Simulated %	100	54	43	41	52	\
LiC 60s1p	-4.7	-6.4	-4.9	-1.0	-4.1	-5.4
Passive HESS	-7.9	-3.0	-1.7	+0.1	-3.0	-1.7

Figure 20 shows the simulation for the passive HESS on an ECMS CS 50%. During the simulation the LiCs' SoC is the reference, and it follows the SoC target of 50%. On the other hand, the battery's SoC is not controlled, and it is progressively discharged, even if the battery maintains the same terminal voltage of the LiCs being in a parallel connection. The graph shows a current that varies very frequently, especially for LiCs. This is also due to the strategy calibration that has been chosen, which could be adjusted to ensure smoother activation profiles. Table 4 shows the fuel consumption results for the ECMS CS 50%. The ECMS guarantees a fuel consumption reduction, but, as in the RBS, the configuration cannot recover all the energy available through regenerative braking due to the control strategy that needs to be adopted for safety reasons, explained in Table 1and Table 2. So, even in this case the results are not as good as the ones obtained through the LiC-only simulation. Moreover, since the system cannot be actively controlled, the capacitor energy cannot be fully used [6,34] as it is bound to the battery voltage.

In conclusion, for the passive HESS, fuel consumption reduction is achieved, but the current limits of the 21700 batteries are too challenging and the passive HESS cannot achieve better recuperation than the LiCs alone. This makes a passive system with a bigger capacity worse than a LiC-only system with respect to fuel consumption reduction.

Semi-Active HESS

The configuration that is here tested is the one based on Figure 18 and on the theory presented in DC-DC Converter.

RBS

The RBS makes the vehicle work in electric drive mode once the SoC is over a certain target value. The current system is characterized by two energy storage systems, and the LiCs' SoC represents the strategy reference. This allows to activate the hybrid components only when the electric traction power is available. On the other side, as it was described in [31,54] the battery deals with the average power and it is charged or discharged until it reaches its limits as it can be seen in Figure 21 and Table 5.

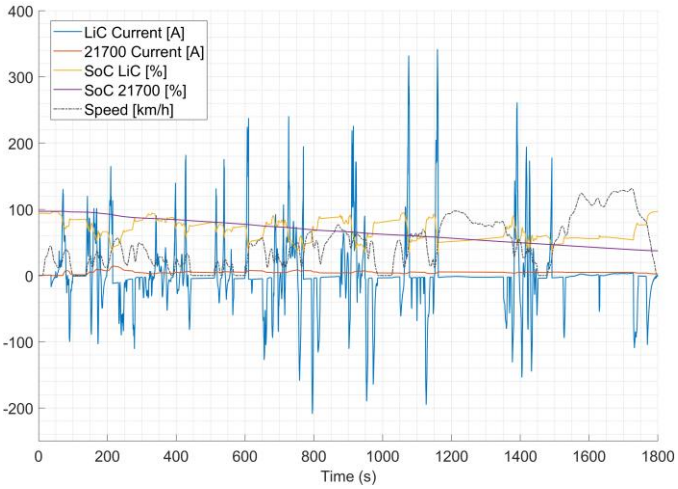

Figure 21. RBS simulation for a semi-active configuration.

Table 5. WLTC Class 3b simulated results, for a P2-P4 hybrid configuration with a passive and a semi-active HESS, and an RBS.

P2-P4 RBS	Phase 1	Phase 2	Phase 3	Phase 4	Combined	Corrected
Simulated %	100	54	43	41	52	\
LiC 60s1p	-1.2	-7.1	-2.7	+0.6	-2.3	\
Passive HESS	-2.1	+1.5	-3.5	+1.2	-0.7	-0.2
Semi-Active HESS	-1.9	-7.1	-5.1	+1.0	-3.0	+0.7

Figure 21 shows the activation of the RBS on the semi-active configuration. The LiCs' SoC is the reference, and the phases in which it is rapidly discharged correspond to the electrical driving activation. With respect to the passive HESS, the electrical driving is here activated more frequently. This is because the semi-active HESS separates the current limits of the two different energy storages, allowing the HESS to react better at dynamic situations. This means also that better recuperation can be achieved without the same strict limits on currents that are present for passive HESS. However, the semi-active configuration is not proficient for fuel economy, as shown in Table 5. This is true once the fuel consumption correction is applied, as the battery is discharged in an uncontrolled manner and ends the cycle at a SoC much lower than the initial one. It can be noticed that even if the RBS guarantees a fuel consumption reduction for the LiC-based hybrid powertrain and for the passive HESS, it is not capable to guarantee the same results for a semi-active HESS.

So, the additional energy present in the form of additional batteries does not guarantee improvements on this side. Different solutions could be analyzed for a HESS with a larger battery pack, that could compensate for the additional weight by extending the driving periods

in electrical drive. Further analysis could be carried out by actuating a control on the battery SoC, in addition to the control already done on the LiCs' SoC.

ECMS

The ECMS is focused on optimizing the equivalent fuel consumption at every instant. The LiCs' SoC is taken as a reference for the strategy, and it follows the SoC target throughout the whole cycle. On the other side, the battery is charged or discharged with respect to the average power. The results for a ECMS in charge sustaining mode are shown in Figure 22 and Table 6.

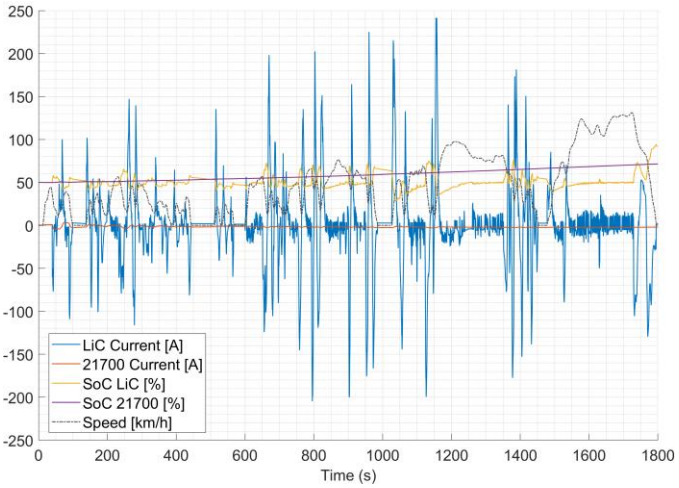

Figure 22. ECMS CS simulation for a semi-active configuration.

Table 6. WLTC Class 3b simulated results, for a P2-P4 hybrid configuration with a passive and a semi-active HESS, and an ECMS CS.

P2-P4 ECMS CS	Phase 1	Phase 2	Phase 3	Phase 4	Combined	Corrected
Simulated %	100	54	43	41	52	\
LiC 60s1p	-4.7	-6.4	-4.9	-1.0	-4.1	-5.4
Passive HESS	-3.6	-1.8	-1.2	+0.3	-1.5	-1.7
Semi-Active HESS	-4.2	-5.3	-3.9	+0.3	-3.1	-6.8

Figure 22 shows that the battery's SoC increases during the cycle, and this leads to a final SoC higher than the initial one. So, the fuel reduction correction is applied. The application of an ECMS CS on a semi-active system is proficient for fuel economy. Differently from the RBS, the ECMS is designed to target the minimization of the equivalent fuel consumption at every instant, and this can be seen in the results that have been obtained. Table 6 shows that a semi-active HESS configuration can reduce fuel consumption up to 6.8%, making this solution better than the LiC 60s1p and the passive HESS. The advantage of the semi-active configuration is the major flexibility in the system's control that makes it possible to work better in dynamic situations. However, the drawback is represented by the high complexity and the addition of a component that involves greater weights and dimensions.

Later, an ECMS Spd is tested. The LiCs' SoC follows the target SoC varying with speed, and the battery works with the average power. The results are shown in Figure 23 and Table 7.

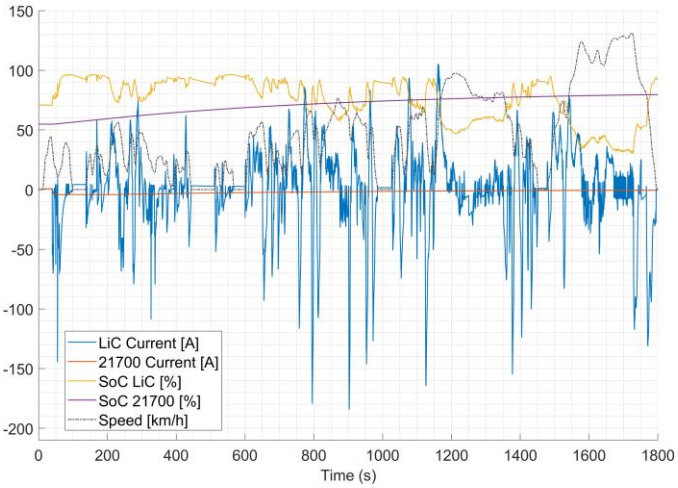

Figure 23. ECMS Spd simulation for a semi-active configuration.

Table 7. WLTC Class 3b simulated results, for a P2-P4 hybrid configuration with a semi-active HESS, and an ECMS Spd.

P2-P4 ECMS Spd	Phase 1	Phase 2	Phase 3	Phase 4	Combined	Corrected
Simulated %	100	54	43	41	52	\
LiC 60s1p	-2.3	-7.9	-5.1	-2.7	-4.3	\
Semi-Active HESS	+2.0	-5.8	-3.6	-1.5	-2.0	-5.5

Figure 23 shows the activation of an ECMS with a SoC target dependent on speed, for a semi-active HESS. The capacity of the semi-active configuration to unbind the two energy storages and the current that is flowing through them, is relevant for this application. In fact, it is thanks to this that the LiCs can follow a rapidly varying SoC target while the battery can deal with the average power, recharging through the entire cycle and acting as an energy reserve whether it would be needed. As shown in Table 7, this configuration guarantees a fuel consumption reduction. This application is of particular interest for super sport cars, as the energy reserve that is guaranteed by the varying SoC target could be used for the activation of additional hybrid control functions. This guarantees great flexibility. and ensures the possibility to follow rapid variations of the target SoC.

Fixed Ratio HESS

The fixed ratio HESS is based on Figure 18 and based on the theory presented in Fixed Ratio DC-DC.

RBS

As for the semi-active configuration, the system is characterized by two energy storage systems, and the LiCs' SoC represents the strategy reference. This allows to activate the electric drive mode only when the traction power, mainly given by the LiCs, is available. On the other side, the battery is controlled by the fixed ratio DC-DC and it is charged or discharged until it reaches its limits as it can be seen in Figure 24 and Table 8.

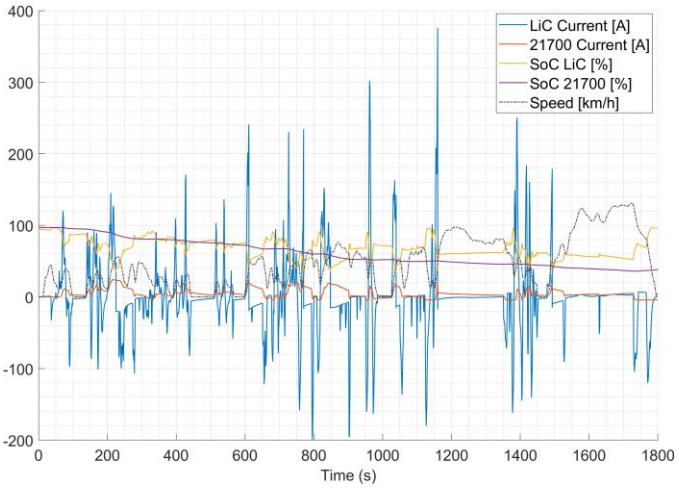

Figure 24. RBS simulation for a fixed ratio configuration.

Table 8. WLTC Class 3b simulated results, for a P2-P4 hybrid configuration with a passive, a semi-active, a fixed-ratio HESS, and an RBS.

P2-P4 RBS	Phase 1	Phase 2	Phase 3	Phase 4	Combined	Corrected
Simulated %	100	54	43	41	52	\
LiC 60s1p	-1.2	-7.1	-2.7	+0.6	-2.3	-2.3
Passive HESS	-2.1	+1.5	-3.5	+1.2	-0.7	-0.2
Semi-Active HESS	-1.9	-7.1	-5.1	+1.0	-3.0	+0.7
Fixed Ratio HESS	-3.1	-8.1	-3.9	+0.9	-3.2	+0.3

The fixed ratio HESS shows a frequent activation of the electrical drive, and it behaves as the semi-active configuration previously simulated. Further analysis should be carried out by actuating a control on the battery SoC, in addition to the control already actuated on the LiCs' SoC. Table 8 shows that the fixed ratio HESS is not capable to achieve a reduction of fuel consumption once the fuel consumption correction is applied to the result.

ECMS

The results for a ECMS in charge sustaining mode are shown in Figure 25 and Table 9.

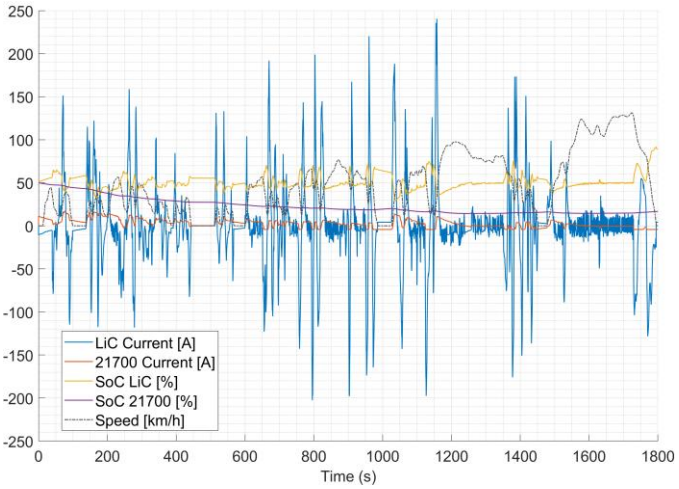

Figure 25. ECMS CS simulation for a fixed ratio configuration.

Table 9. WLTC Class 3b simulated results, for a P2-P4 hybrid configuration with a passive, a semi-active, a fixed-ratio HESS, and an ECMS CS.

P2-P4 ECMS CS	Phase 1	Phase 2	Phase 3	Phase 4	Combined	Corrected
Simulated %	100	54	43	41	52	\
LiC 60s1p	-4.7	-6.4	-4.9	-1.0	-4.1	-5.4
Passive HESS	-3.6	-1.8	-1.2	+0.3	-1.5	-1.7
Semi-Active HESS	-4.2	-5.3	-3.9	+0.3	-3.1	-6.8
Fixed Ratio HESS	-8.3	-7.4	-5.5	-0.1	-5.1	-4.0

The results in Table 9 show that the fixed ratio HESS configuration guarantees fuel consumption reduction when simulated on an ECMS CS 50%. This makes the fixed ratio HESS a viable solution for fuel economy. However, the control simplicity of the fixed-ratio DC-DC is here paid with worse results with respect to the semi-active configuration. At last, an ECMS Spd is tested. The LiCs' SoC follows the target SoC that varies with speed. The results are shown in Figure 26 and Table 10.

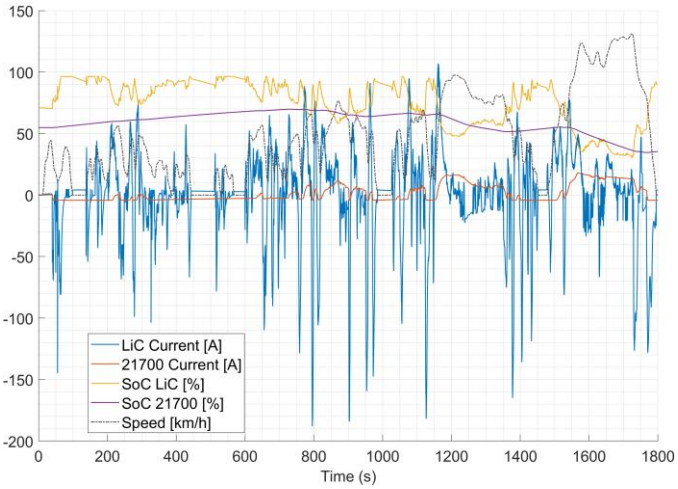

Figure 26. ECMS Spd simulation for a fixed ratio configuration.

Table 10. WLTC Class 3b simulated results, for a P2-P4 hybrid configuration with a semi-active, a fixed-ratio HESS, and an ECMS Spd.

P2-P4 ECMS Spd	Phase 1	Phase 2	Phase 3	Phase 4	Combined	Corrected
Simulated %	100	54	43	41	52	\
LiC 60s1p	-2.3	-7.9	-5.1	-2.7	-4.3	\
Semi-Active HESS	+2.0	-5.8	-3.6	-1.5	-2.0	-5.5
Fixed Ratio HESS	+1.7	-8.3	-6.3	-3.1	-3.8	-3.0

Table 9 and Table 10 show that the fixed ratio DC-DC is capable to achieve fuel economy when the hybrid control strategy targets the minimization of equivalent fuel consumption as the ECMS does. However, the results that are obtained do not improve what was previously simulated on the semi-active HESS. The current profiles that are obtained in Figure 26 resemble the ones obtained for the semi-active simulations in Figure 23, especially for the LiCs' current that in both cases is capable to react at the SoC target variations. On the other hand, the battery's current has a different profile as in the semi-active configuration is meant to deal with the average load power, while here aims to maintain the same voltage between battery and load as explained in Fixed Ratio DC-DC.

Performance

The last part of the activity has been destined to the study of dynamic conditions (typically seen for sport driving or use on the track). The energy storage system is here dimensioned to recover all the energy available for high-speed braking. The study aims to understand what kind of solutions would be needed to satisfy this target and whether these solutions are viable. The semi-active fixed ratio HESS is now analyzed for performance. Simulations for a 0-200 km/h acceleration and a 200-0 km/h braking are run. At first, a braking from 200 km/h to 0 km/h is analyzed as this represent an extremely challenging condition, especially for the battery due to its stringent current limit. During braking, energy is usually dissipated through mechanical brakes, but here it can be recovered through regenerative braking. The target is to design a HESS capable of storing all the energy generated from braking. The hybrid powertrain as it has been described until now is not capable of recovering the whole amount of energy, so a new HESS is designed.

Since the batteries are strongly limited in current, they are not capable of recovering great energy quantities during hard braking and their impact in a high-power situation, like the 200-0 km/h braking, is low. So, the battery maintains the 54s1p configuration. On the other side, the LiCs are sized to recover all the available energy and a configuration of 60s5p is chosen, maintaining the same voltage range of the previous hybrid configuration. Furthermore, EMs about 5 times more powerful than the previous configuration are chosen to satisfy the peak power. The new hybrid powertrain, which we refer to as Hybrid 60s5p, is simulated as shown in Figure 27.

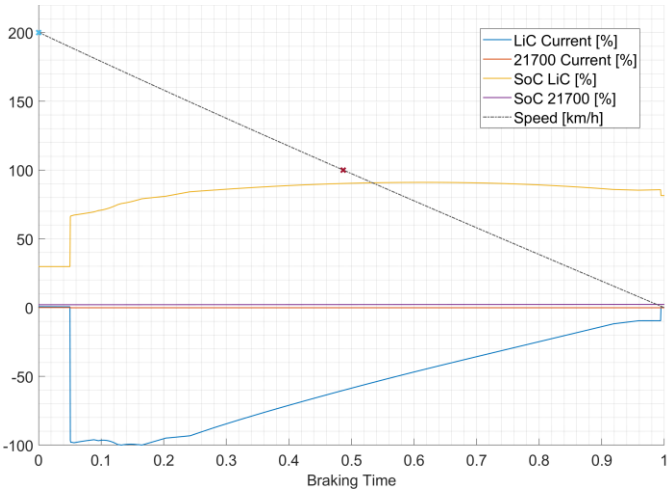

Figure 27. Hybrid 60s5p simulation for the 200-0 km/h braking.

The simulation demonstrated that during recuperation the braking energy is coming from the EMs and not the mechanical brakes, allowing to recover all the available energy. In this simulation the battery and the LiCs are starting at the same voltage (respectively corresponding to a LiCs SoC=30% and a battery SoC=2%), and, as soon as the vehicle speed gets under 190 km/h, the regenerative braking strategy is activated as the front EM is attached.

A negative current start flowing in the HESS, and the battery immediately reaches its lower limit while the LiCs can manage all the remaining current (here the values are normalized with respect to the maximum LiCs' current). The SoC [%] in Figure 27 of a pack of capacitors at terminal voltage V_t, minimum voltage V_{min}, maximum voltage V_{max}, is equal to:

$$SoC = \left(\frac{{V_t}^2 - {V_{min}}^2}{{V_{max}}^2 - {V_{min}}^2} \right) \cdot 100 \quad (26)$$

Meaning that it depends on the terminal voltage of the LiCs' pack, that according to the scheme in Figure 5 is formulated as:

$$V_t = V_c - i_c \cdot R_c \quad (27)$$

This means that its variation depends both on the internal voltage that increases during a braking simulation, and on the voltage drop generated by the negative current. This is evident at the beginning of the simulation (approximately instant 0.05), when a rapid spike takes place because of the sudden demand of current. Moreover, this explains the curvilinear pattern of the SoC during the braking phase.

As the braking phase ends, the current goes back to zero and the system is left with a voltage imbalance between LiCs and batteries. The two components start exchanging low values of current to bridge this gap and the LiCs start delivering positive current to the battery until voltage equilibrium is reached. This is shown in Figure 28, where the LiCs current becomes positive and the SoC of the batteries slowly increases to reach the same LiCs voltage as explained in Fixed Ratio DC-DC.

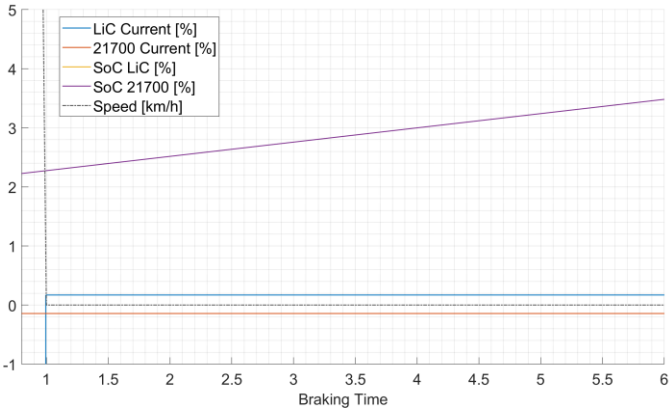

Figure 28. Detail of the system's currents.

Figure 29 shows the energy dissipated through mechanical braking. The Hybrid 60s5p makes use of the mechanical brake mainly in the initial phase as the regenerative braking is activated under 190 km/h. The remaining braking energy is almost completely given by regenerative braking, meaning that the HESS is properly sized.

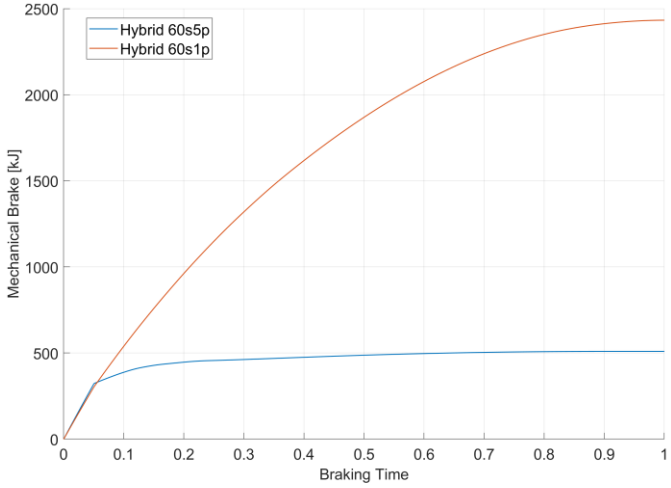

Figure 29. Mechanical contribution for the 200-0 km/h braking.

The Hybrid 60s5p is tested also for a 0-200 km/h acceleration. At first, the conventional vehicle is simulated for a 0-200 km/h acceleration and

the times of 0-100 km/h, and 0-200 km/h are recorded and normalized with respect to the greatest of the two. Later, simulations for the Hybrid 60s1p and for the Hybrid 60s5p are run and the results are compared to the conventional ones, showing the percentage improvement or reduction, as shown in Table 11, Figure 30, and Figure 31.

Table 11. 0- 200 km/h simulated performance results.

Time	0-100 km/h	0-200 km/h
Conventional (%)	36	100
Hybrid 60s1p (%)	+15	+6
Hybrid 60s5p (%)	-14	-25

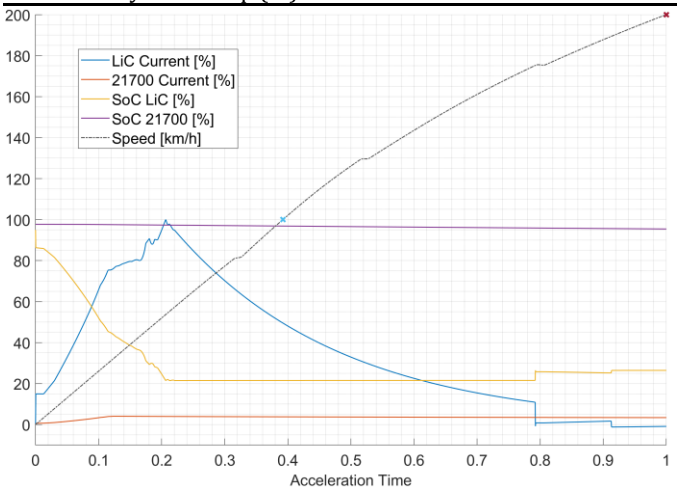

Figure 30. Hybrid 60s1p simulation for the 0-200 km/h acceleration.

The Hybrid 60s1p is less performant than the conventional vehicle. This is because in hybrid configuration the P4 EM is the only power source at the front axle, and it is not capable to output the same power that was split to the front from the ICE in conventional configuration all-wheel drive. Moreover, as soon as the LiCs reach the minimum SoC, the hybrid contribution ends leaving the ICE alone. In fact, the battery is not capable to satisfy the power request by itself. As the hybrid contribution ends, the battery continues to deliver positive current to the LiCs, as the HESS tries to bridge the difference in voltage between the LiCs and the battery.

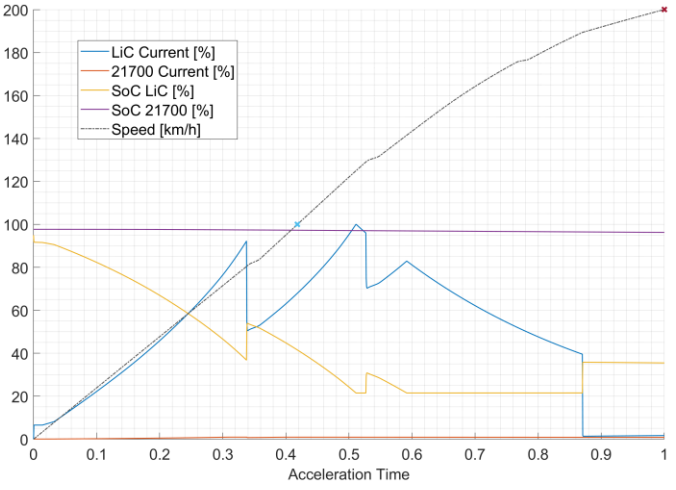

Figure 31. Hybrid 60s5p simulation for the 0-200 km/h acceleration.

In Figure 31, at approximately instant 0.87, the vehicle speed of 190km/h is reached, and the front EM is detached modifying the current requests. In the Hybrid 60s5p configuration the front EM delivers more power than before and the LiCs deliver higher currents. Moreover, the presence of parallels lowers the internal resistance and the voltage drop, and this allows to run in hybrid mode for longer time.

The results highlight that a HESS can guarantee improvements on the 0-200 km/h acceleration and energy recuperation on the 200-0 km/h braking. While the battery can be seen as the responsible for the energy target, the LiCs are capable to achieve the power target. Performance tests highlight the possibility of using a HESS to achieve both power and energy targets, focusing on proper LiCs and battery sizing.

Conclusions

The present document carries out the analysis of a super sport car HEV fitted with two EMs in P2-P4 configuration and with a HESS based on LiCs and Li-Ion batteries. The control strategies that are adopted to simulate this vehicle configuration are an RBS and an ECMS. At first, the HESS is introduced as a passive HESS, where the LiCs and batteries are directly connected in parallel. Then, a semi-active HESS is introduced, where a DC-DC converter is the interface for the two energy storage systems. The DC-DC converter is also evaluated as a fixed ratio DC-DC. The control strategy that is adopted for the semi-active HESS is an online energy management strategy capable to guarantee real-time performance.

The current work is based on experimentally validated models, and the main contribution is represented by the evaluations that can be made by integrating the systems in a super sport HEV. The various energy storage configurations that are analyzed and simulated on the WLTC Class 3b have their own advantages and disadvantages. The passive HESS is a simple system that ensures low weight and small size; however, it cannot be actively controlled, and it limits the energy that would be available from LiCs. The results for the passive HESS show a low reduction in fuel consumption (up to 1.7% with an ECMS), and a strong limit in the energy that could be recovered because of the current limits.

On the other side, by introducing a DC-DC converter, the semi-active HESS increases the weight, size, and complexity. However, it allows to properly control the currents flowing in both batteries and LiCs guaranteeing lower stress on the batteries and better energy recuperation. The semi-active configuration does not achieve fuel economy with the RBS but guarantees a fuel consumption reduction that goes up to 6.8% for the ECMS. This highlights the opportunity to achieve better results through an optimization of the control strategies.

The adoption of a fixed ratio DC-DC converter is seen as an alternative to maintain the complexity low, while still controlling the current limits of the HESS. This simplicity is paid with worse results on fuel economy, if compared with the other semi-active configuration, both for an RBS and an ECMS.

Another consideration is related to the comparison between the HESS and an energy storage uniquely based on LiCs. The choice to work with a HESS allows to improve the system's flexibility, as greater energy content could be guaranteed, while maintaining the power of the LiCs. However, the results for the RBS show that in some situations, the energy storage system uniquely based on LiCs could achieve better fuel economy results. On one side, this clarifies the importance of high-power density systems for super sports car, that can guarantee fuel economy even if characterized by low energy density. On the other side, it makes clear that the hybrid system carries more weight and that it needs a more accurate management of the additional energy that it makes available (for example with strategies targeting the minimization of fuel consumption), which otherwise will not lead to the expected benefits. However, the main limit of the configuration is represented by the batteries' current limit, that impacts on the whole

system. With respect to this, the introduction of high-power batteries could be prioritized.

The final analysis on the super sport HEV is run by simulating its performance on fast accelerations and decelerations. A HESS is specifically sized to recover all the energy available during a 200-0 km/h braking and to guarantee a reduction in the time performance for a 0-100 km/h and 0-200 km/h acceleration. These simulations show that the HESS can be an interesting solution to cover both the energy and power requirements that are typically associated to a super sport HEV.

To sum up, it is evident that the LiC technology is limited for energy performance at the moment, but with a proper development of the control strategy and keeping into account the growth of the technology [15,63–65], the system capabilities could lead to major applications in the hybrid environment. The high-power characteristic of the LiCs makes them interesting for applications like super sport cars, which greatly evaluate features such as performance and drivability along with fuel economy.

References

1. Watzenig, D. and Brandstätter, B., eds., "Comprehensive Energy Management – Eco Routing & Velocity Profiles," Springer International Publishing, Cham, ISBN 978-3-319-53164-9, 2017, doi:10.1007/978-3-319-53165-6.
2. Olin, P., Aggoune, K., Tang, L., Confer, K., Kirwan, J., Rajakumar Deshpande, S., Gupta, S., Tulpule, P., Canova, M., and Rizzoni, G., "Reducing Fuel Consumption by Using Information from Connected and Automated Vehicle Modules to Optimize Propulsion System Control," *SAE Technical Paper*, 2019-01–1213, 2019, doi:10.4271/2019-01-1213.
3. Zhao, Y., Song, H., Liu, Y., and Yu, Z., "Energy Management of Dual Energy Source of Hydrogen Fuel Cell Hybrid Electric Vehicles," *SAE Technical Paper*, 2020-01–0595, 2020, doi:10.4271/2020-01-0595.
4. Jeffers, M.A., Miller, E., Kelly, K., Kresse, J., Li, K., Dalton, J., Kader, M., and Frazier, C., "Development and Demonstration of a Class 6 Range-Extended Electric Vehicle for Commercial Pickup and Delivery Operation," *SAE Technical Paper*, 2020-01–0848, 2020, doi:10.4271/2020-01-0848.
5. Jager, B. de, Keulen, T. van, and Kessels, J., "Optimal Control of Hybrid Vehicles," Springer London, London, ISBN 978-1-4471-5075-6, 2013, doi:10.1007/978-1-4471-5076-3.
6. Ehsani, M., ed., "Modern electric, hybrid electric, and fuel cell vehicles: fundamentals, theory, and design," CRC Press, Boca Raton, ISBN 978-0-8493-3154-1, 2005.
7. Caramia, G., "Modelling and Optimization of Energy Management Strategies for Hybrid Vehicles," Dissertation Thesis, Università di Bologna, 2020.
8. Emadi, A., ed., "Handbook of automotive power electronics and motor drives," Taylor & Francis, Boca Raton, ISBN 978-0-8247-2361-3, 2005.
9. Onori, S., Serrao, L., and Rizzoni, G., "Hybrid Electric Vehicles," Springer London, London, ISBN 978-1-4471-6779-2, 2016, doi:10.1007/978-1-4471-6781-5.
10. Aravindan, V., Gnanaraj, J., Lee, Y.-S., and Madhavi, S., "Insertion-Type Electrodes for Nonaqueous Li-Ion Capacitors," *Chem. Rev.* 114(23):11619–11635, 2014, doi:10.1021/cr5000915.
11. Sheberla, D., Bachman, J.C., Elias, J.S., Sun, C.-J., Shao-Horn, Y., and Dincă, M., "Conductive MOF electrodes for stable supercapacitors with high areal capacitance," *Nature Mater* 16(2):220–224, 2017, doi:10.1038/nmat4766.
12. Bi, S., Banda, H., Chen, M., Niu, L., Chen, M., Wu, T., Wang, J., Wang, R., Feng, J., Chen, T., Dincă, M., Kornyshev, A.A., and Feng, G., "Molecular understanding of charge storage and charging dynamics in supercapacitors with MOF electrodes and ionic liquid electrolytes," *Nat. Mater.* 19(5):552–558, 2020, doi:10.1038/s41563-019-0598-7.
13. Ronsmans, J. and Lalande, B., "Combining energy with power: Lithium-ion capacitors," *2015 International Conference on Electrical Systems for Aircraft, Railway, Ship Propulsion and Road Vehicles (ESARS)*, 1–4, 2015, doi:10.1109/ESARS.2015.7101494.
14. BU-107: Comparison Table of Secondary Batteries, https://batteryuniversity.com/article/bu-107-comparison-table-of-secondary-batteries, 2010.
15. Valmra, E., "A New Approach for Ultracapacitor-Battery Hybrid Energy Storage Solutions," *International Workshop on Supercapacitor and Energy Storage*, Skeleton Technologies GmbH, Bologna, 2019.
16. Burke, A. and Miller, M., "The power capability of ultracapacitors and lithium batteries for electric and hybrid vehicle applications," *Journal of Power Sources* 196(1):514–522, 2011, doi:10.1016/j.jpowsour.2010.06.092.
17. Xun, Q., Liu, Y., and Holmberg, E., "A Comparative Study of Fuel Cell Electric Vehicles Hybridization with Battery or Supercapacitor," *2018 International Symposium on Power Electronics, Electrical Drives, Automation and Motion (SPEEDAM)*, IEEE, Amalfi, ISBN 978-1-5386-4941-1: 389–394, 2018, doi:10.1109/SPEEDAM.2018.8445386.
18. Thounthong, P., Chunkag, V., Sethakul, P., Davat, B., and Hinaje, M., "Comparative Study of Fuel-Cell Vehicle Hybridization with Battery or Supercapacitor Storage Device," *IEEE Trans. Veh. Technol.* 58(8):3892–3904, 2009, doi:10.1109/TVT.2009.2028571.
19. Gao, Y., Moghbelli, H., Ehsani, M., Frazier, G., Kajs, J., and Bayne, S., "Investigation of High-Energy and High-Power Hybrid Energy Storage Systems for Military Vehicle Application," SAE Technical Paper: 2003-01–2287, 2003, doi:10.4271/2003-01-2287.
20. Nagai, H., Morita, M., and Satoh, K., "Development of the Li-ion Battery Cell for Hybrid Vehicle," *SAE Technical Paper*, 2016-01–1207, 2016, doi:10.4271/2016-01-1207.
21. Rahmani, F., Niknejad, P., Agarwal, T., and Barzegaran, M., "Gallium Nitride Inverter Design with Compatible Snubber Circuits for Implementing Wireless Charging of Electric Vehicle Batteries," *Machines* 8(3):56, 2020, doi:10.3390/machines8030056.
22. Liu, W., "Hybrid electric vehicle system modeling and control," 2nd edition, Wiley, Chichester, West Sussex, UK ; Hoboken, NJ, USA, ISBN 978-1-119-27894-8, 2017.
23. Shah, V.A., Karndhar, S.G., Maheshwari, R., Kundu, P., and Desai, H., "An energy management system for a battery ultracapacitor Hybrid Electric Vehicle," *2009 International Conference on Industrial and Information Systems (ICIIS)*, IEEE, Peradeniya, Sri Lanka, ISBN 978-1-4244-4836-4: 408–413, 2009, doi:10.1109/ICIINFS.2009.5429825.
24. Kumar, S. and Ikkurti, H.P., "Design and control of novel power electronics interface for battery-ultracapacitor hybrid energy storage system," *International Conference on Sustainable Energy and Intelligent Systems (SEISCON 2011)*, IET, Chennai, India, ISBN 978-93-80430-00-3: 236–241, 2011, doi:10.1049/cp.2011.0367.
25. Walvekar, A.S., Bhateshvar, Y.K., and Vora, K., "Active Hybrid Energy Storage System for Electric Two Wheeler," *SAE Technical Paper 2020-28-0516*, 2020, doi:10.4271/2020-28-0516.
26. Aharon, I. and Kuperman, A., "Topological Overview of Powertrains for Battery-Powered Vehicles With Range Extenders," *IEEE Trans. Power Electron.* 26(3):868–876, 2011, doi:10.1109/TPEL.2011.2107037.

27. Kuperman, A. and Aharon, I., “Battery–ultracapacitor hybrids for pulsed current loads: A review,” *Renewable and Sustainable Energy Reviews* 15(2):981–992, 2011, doi:10.1016/j.rser.2010.11.010.
28. Lerman, C., Horosov, A., and Kuperman, A., “Capacitor semi-active battery-ultracapacitor hybrid energy source,” *2012 IEEE 27th Convention of Electrical and Electronics Engineers in Israel*, IEEE, Eilat, Israel, ISBN 978-1-4673-4681-8: 1–4, 2012, doi:10.1109/EEEI.2012.6377027.
29. Aharon, I. and Kuperman, A., “Design of semi-active battery-ultracapacitor hybrids,” *2010 IEEE 26-th Convention of Electrical and Electronics Engineers in Israel*, IEEE, Eilat, Israel, ISBN 978-1-4244-8681-6: 000593–000597, 2010, doi:10.1109/EEEI.2010.5662148.
30. Seim, L.H., “Modeling, control and experimental testing of a supercapacitor/battery hybrid system : passive and semi-active topologies,” Norwegian University of Life Sciences, Department of Mathematical Sciences and Technology, 2012.
31. Gao, L., Dougal, R.A., and Liu, S., “Power Enhancement of an Actively Controlled Battery/Ultracapacitor Hybrid,” *IEEE Trans. Power Electron.* 20(1):236–243, 2005, doi:10.1109/TPEL.2004.839784.
32. Neenu, M. and Muthukumaran, S., “A battery with ultra capacitor hybrid energy storage system in electric vehicles,” *IEEE-International Conference On Advances In Engineering, Science And Management (ICAESM -2012)*, 731–735, 2012.
33. Chuan, Y., Mi, C., and Zhang, M., “Comparative Study of a Passive Hybrid Energy Storage System Using Lithium Ion Battery and Ultracapacitor,” *WEVJ* 5(1):83–90, 2012, doi:10.3390/wevj5010083.
34. Dougal, R.A., Liu, S., and White, R.E., “Power and life extension of battery-ultracapacitor hybrids,” *IEEE Trans. Comp. Packag. Technol.* 25(1):120–131, 2002, doi:10.1109/6144.991184.
35. Villa, A. and Piegari, L., “Impiego di supercondensatori in parallelo a batterie per estendere l’autonomia di veicoli elettrici a basse temperature,” Politecnico di Milano, Scuola di Ingegneria Industriale e dell’Informazione, Corso di Laurea in Ingegneria Elettrica, 2016.
36. Where fixed-ratio converters fit in high-power delivery systems - Power Electronic Tips, https://www.powerelectronictips.com/where-fixed-ratio-converters-fit-in-high-power-delivery-systems-faq/, May 2021.
37. Mukherjee, S., Kumar, A., and Chakraborty, S., “Comparison of DAB and *LLC* DC–DC Converters in High-Step-Down Fixed-Conversion-Ratio (DCX) Applications,” *IEEE Trans. Power Electron.* 36(4):4383–4398, 2021, doi:10.1109/TPEL.2020.3019796.
38. Salato, M., “A novel approach to industrial rectifier systems: dense, efficient and modular architecture enabled by fixed-ratio bus converters,” *Power Solution Brief, Vicor*, 2014.
39. Salmasi, F.R., “Control Strategies for Hybrid Electric Vehicles: Evolution, Classification, Comparison, and Future Trends,” *IEEE Transactions on Vehicular Technology* 56(5):2393–2404, 2007, doi:10.1109/TVT.2007.899933.
40. Cerofolini, A., “Optimal Supervisory Control of Hybrid Vehicles,” Dissertation Thesis, Università di Bologna, 2014, doi:10.6092/unibo/amsdottorato/6357.
41. Böhme, T.J. and Frank, B., “Hybrid Systems, Optimal Control and Hybrid Vehicles: Theory, Methods and Applications,” Springer International Publishing, Cham, ISBN 978-3-319-51315-7, 2017, doi:10.1007/978-3-319-51317-1.
42. Chao Sun, Xiaosong Hu, Moura, S.J., and Fengchun Sun, “Velocity Predictors for Predictive Energy Management in Hybrid Electric Vehicles,” *IEEE Trans. Contr. Syst. Technol.* 23(3):1197–1204, 2015, doi:10.1109/TCST.2014.2359176.
43. Trovão, J.P., Pereirinha, P.G., Jorge, H.M., and Antunes, C.H., “A multi-level energy management system for multi-source electric vehicles – An integrated rule-based meta-heuristic approach,” *Applied Energy* 105:304–318, 2013, doi:10.1016/j.apenergy.2012.12.081.
44. Zhang, Q. and Li, G., “Experimental Study on a Semi-Active Battery-Supercapacitor Hybrid Energy Storage System for Electric Vehicle Application,” *IEEE Transactions on Power Electronics* 35(1):1014–1021, 2020, doi:10.1109/TPEL.2019.2912425.
45. Schouten, N.J., Salman, M.A., and Kheir, N.A., “Energy Management Strategies for Parallel Hybrid Vehicles Using Fuzzy Logic,” *IFAC Proceedings Volumes* 33(26):83–88, 2000, doi:10.1016/S1474-6670(17)39125-5.
46. Song, Z., Hofmann, H., Li, J., Han, X., and Ouyang, M., “Optimization for a hybrid energy storage system in electric vehicles using dynamic programing approach,” *Applied Energy* 139:151–162, 2015, doi:10.1016/j.apenergy.2014.11.020.
47. Ramoul, J., Chemali, E., Dorn-Gomba, L., and Emadi, A., “A Neural Network Energy Management Controller Applied to a Hybrid Energy Storage System using Multi-Source Inverter,” *2018 IEEE Energy Conversion Congress and Exposition (ECCE)*, 2741–2747, 2018, doi:10.1109/ECCE.2018.8558326.
48. Shen, J. and Khaligh, A., “A Supervisory Energy Management Control Strategy in a Battery/Ultracapacitor Hybrid Energy Storage System,” *IEEE Transactions on Transportation Electrification* 1(3):223–231, 2015, doi:10.1109/TTE.2015.2464690.
49. Xiong, R., Cao, J., and Yu, Q., “Reinforcement learning-based real-time power management for hybrid energy storage system in the plug-in hybrid electric vehicle,” *Applied Energy* 211:538–548, 2018, doi:10.1016/j.apenergy.2017.11.072.
50. Chen, Z., Hu, H., Wu, Y., Xiao, R., Shen, J., and Liu, Y., “Energy Management for a Power-Split Plug-In Hybrid Electric Vehicle Based on Reinforcement Learning,” *Applied Sciences* 8(12):2494, 2018, doi:10.3390/app8122494.
51. Chen, H., Xiong, R., Lin, C., and Shen, W., “Model predictive control based real-time energy management for hybrid energy storage system,” *CSEE Journal of Power and Energy Systems* 7(4):862–874, 2021, doi:10.17775/CSEEJPES.2020.02180.
52. Franceschi, A., Cavina, N., Parenti, R., Reggiani, M., and Corti, E., “Modeling, Validation and Control Strategy Development of a Hybrid Super Sport Car Based on Lithium Ion Capacitors,” SAE Technical Paper: 2020-01–0442, 2020, doi:10.4271/2020-01-0442.
53. Franceschi, A., Cavina, N., Parenti, R., Reggiani, M., and Corti, E., “Energy Management Optimization of a Dual Motor Lithium Ion Capacitors-Based Hybrid Super Sport Car,” *Applied Sciences* 11(2):885, 2021, doi:10.3390/app11020885.
54. Gao, L., Dougal, R.A., and Liu, S., “Active power sharing in hybrid battery/capacitor power sources,” *Eighteenth Annual IEEE Applied Power Electronics Conference and Exposition, 2003. APEC ’03.*, IEEE, Miami Beach, FL, USA, ISBN 978-0-7803-7768-4: 497–503, 2003, doi:10.1109/APEC.2003.1179259.
55. Zubieta, L. and Bonert, R., “Characterization of double-layer capacitors for power electronics applications,” *IEEE Transactions on Industry Applications* 36(1):199–205, 2000, doi:10.1109/28.821816.
56. INR-21700-P42A – Molicel, http://www.molicel.com/product/inr-21700-p42a/, Apr. 2021.
57. Yao, L.W., Aziz, J.A., Kong, P.Y., and Idris, N.R.N., “Modeling of lithium-ion battery using MATLAB/simulink,” *IECON 2013 - 39th Annual Conference of the IEEE Industrial Electronics Society*, IEEE, Vienna, Austria, ISBN 978-1-4799-0224-8: 1729–1734, 2013, doi:10.1109/IECON.2013.6699393.

58. Ahmed, R., Gazzarri, J., Onori, S., Habibi, S., Jackey, R., Rzemien, K., Tjong, J., and LeSage, J., "Model-Based Parameter Identification of Healthy and Aged Li-ion Batteries for Electric Vehicle Applications," *SAE Int. J. Alt. Power.* 4(2):233–247, 2015, doi:10.4271/2015-01-0252.
59. Addendum 15: Global technical regulation No. 15, Worldwide harmonized Light vehicles Test Procedure, Established in the Global Registry on 12 March 2014, United Nations.
60. Ma, T., Yang, H., and Lu, L., "Development of hybrid battery–supercapacitor energy storage for remote area renewable energy systems," *Applied Energy* 153:56–62, 2015, doi:10.1016/j.apenergy.2014.12.008.
61. Lukic, S.M., Wirasingha, S.G., Rodriguez, F., Cao, J., and Emadi, A., "Power Management of an Ultracapacitor/Battery Hybrid Energy Storage System in an HEV," *2006 IEEE Vehicle Power and Propulsion Conference*, IEEE, Windsor, UK, ISBN 978-1-4244-0158-1: 1–6, 2006, doi:10.1109/VPPC.2006.364357.
62. Cao, J. and Emadi, A., "A new battery/ultra-capacitor hybrid energy storage system for electric, hybrid and plug-in hybrid electric vehicles," *2009 IEEE Vehicle Power and Propulsion Conference*, 941–946, 2009, doi:10.1109/VPPC.2009.5289744.
63. Faraji, S. and Ani, F.N., "The development supercapacitor from activated carbon by electroless plating—A review," *Renewable and Sustainable Energy Reviews* 42:823–834, 2015, doi:10.1016/j.rser.2014.10.068.
64. Raza, W., Ali, F., Raza, N., Luo, Y., Kim, K.-H., Yang, J., Kumar, S., Mehmood, A., and Kwon, E.E., "Recent advancements in supercapacitor technology," *Nano Energy* 52:441–473, 2018, doi:10.1016/j.nanoen.2018.08.013.
65. Muzaffar, A., Ahamed, M.B., Deshmukh, K., and Thirumalai, J., "A review on recent advances in hybrid supercapacitors: Design, fabrication and applications," *Renewable and Sustainable Energy Reviews* 101:123–145, 2019, doi:10.1016/j.rser.2018.10.026.

Definitions/Abbreviations

CO2	Carbon Dioxide
CS	Charge Sustaining
ECMS	Equivalent Consumption Minimization Strategy
EM	Electric Motor
EV	Electric Vehicle
HESS	Hybrid Energy Storage System
HEV	Hybrid Electric Vehicle
ICE	Internal Combustion Engine
LiC	Lithium-Ion Capacitor
PDT	Pulsed Discharge Test
RBS	Rule Based Strategy
SoC	State of Charge
WLTC	Worldwide harmonized Light-duty vehicles Test Cycle